Mineralium Deposita (2024) 59:373–396
https://doi.org/10.1007/s00126-023-01214-7

ARTICLE

Post-Archean Nb-REE-U enrichment in the Superior craton recorded in metasomatised mantle rocks erupted in the 1.1 Ga Midcontinental Rift event

Hélène Legros[1] · Janina Czas[1] · Yan Luo[1] · Sarah Woodland[1] · Chiranjeeb Sarkar[1] · Steven B. Shirey[2] · Dan Schulze[3] · D. Graham Pearson[1]

Received: 8 March 2023 / Accepted: 8 September 2023 / Published online: 30 September 2023

Abstract

Mantle xenoliths in a Mesoproterozoic lamprophyre dyke at Elliot Lake, Ontario, located on the east margin of the Midcontinent Rift (MCR), erupted at ~ 1.1 Ga. These xenoliths enable a study of critical metal enrichment in the sub-cratonic lithospheric mantle (SCLM). Whole-rock major and trace element data from a suite of peridotite xenoliths document a combination of melt depletion and cryptic metasomatic processes. Trace element whole-rock and mineral systematics show a specific endowment in Nb-U-REE (ca. 5–30 ppm mean value), linked to carbonated silicate metasomatism. Geochronological data from the lamprophyre host (Rb–Sr age of 1112.8 ± 4.95 Ma) and the mantle xenoliths (Re-Os) indicate that our samples document the state of the mantle during the earlier stages of magmatism of the MCR. Mineral thermobarometry reveals a hot geotherm reflecting the thinning of the Superior cratonic root to 110 km. Most of the Nb-U-REE deposits and anomalies associated with the MCR event are located around Lake Superior. Here we document for the first time north of Lake Huron, metasomatic processes in the lithosphere that may have created Nb-U-REE metal endowment. The mantle events documented here relate to other observations made in the Slave and North China craton and show how silico-carbonated mid-lithospheric metasomatism up-grades the cratonic lithospheric mantle into a fertile source. Comparison with other small degree melts such as kimberlites, and mantle metasomes related to the MARID suite, show that small degree melts are very efficient at transporting critical metals from the HFSE group plus U and Th, into Earth's lithosphere.

Keywords Critical metals · REE · Elliot Lake · Superior craton · Metasomatism · Mantle lithosphere

Introduction

Exploration for critical metals is constantly increasing due to today's high demand for new technologies. Cratons and lithospheric margins have been recognized to be favorable reservoirs for critical metals and are a host to giant mineral deposits and mineral provinces (Groves and Santosh 2021). While there has been increased focus on critical metal deposits in the crustal section of cratons, little study has been made on the potential metal reservoirs of the sub-cratonic lithospheric mantle (SCLM), the enrichment in critical metals in this reservoir (e.g. Veglio et al. 2022), and the magmas transporting them to the surface (Griffin et al. 2013).

Mantle metasomatism has been advocated as a potential enrichment process linked to the formation of a wide variety of ore deposits such as gold, VMS, and diamonds in the Slave craton in Canada (Geusebroek and Duke 2004; Bussweiler et al. 2018; Lougheed et al. 2020). However, despite the considerable metal potential of the Superior craton of eastern Canada (Percival et al. 2012), few studies have tried to link mantle metal enrichment with crustal ore potential in that area until the recent work of Lawley et al. (2018).

A key event in the history of the southern Superior craton is the formation of the Midcontinent Rift (MCR), located

Editorial handling: M. Fayek

✉ Hélène Legros
helene.legros@mern.gouv.qc.ca

[1] Department of Earth and Atmospheric Sciences, University of Alberta, Edmonton, AB T6G 2E3, Canada

[2] Earth & Planets Laboratory, Carnegie Science, 5241 Broad Branch Road, NW, Washington, DC 20015, USA

[3] Department of Earth Sciences and Department of Chemical and Physical Sciences, University of Toronto, Mississauga, ON L5L 1C6, Canada

south of the Superior craton. The MCR is one of the best preserved Proterozoic intra-continental rifts and hosts a wide variety of critical metal deposits associated with the Keweenawan large igneous province (LIP) (Heaman et al. 2007; Smyk and Franklin 2007; Miller et al. 2013). Most of the MCR-related deposits are located in the center of the rift, around Lake Superior (Woodruff et al. 2020). However, this region has also been extensively overprinted by subsequent magmatism and hydrothermal processes (Good et al. 2021). Therefore, the Elliot Lake area in Ontario located on the east rift margin, which was less impacted by post-MCR processes, represents an ideal location to conduct an initial study of critical metal enrichment in the southern Superior cratonic mantle at that time. The Elliot Lake samples are a good example of magmatism carrying pieces of continental lithosphere to the surface that may have been variably affected by metasomatic processes associated with the MCR. The Elliot Lake area has received significant attention for its uranium mining activities as well as its minor resources of gold, REE, and Ni-Cu-PGE (Martindale 1968; Robinson and Spooner 1982; Castor 2008). However, no studies have yet described the lithospheric mantle underpinning this area. Here we report new major and trace element data on whole-rock powders and single minerals from a suite of peridotite xenoliths, as well as new geochronology results on the mantle samples and their lamprophyre host. Our aim is to assess the extent and style of metasomatism in the lithospheric mantle below the regional ore deposits and investigate the links between crust and mantle metal enrichments in the southern Superior lithosphere during the MCR event.

Regional geological setting

The Elliot Lake area is located north of Lake Huron and ~ 100 km southwest of the Sudbury basin, in Ontario, Canada (Fig. 1). Outcropping rocks in the area belong to the Wawa-Abitibi Terrane and include the Superior Archean basement, several pulses of Archean mafic and ultramafic intrusive rocks, and the Paleoproterozoic Huronian Supergroup (Robertson 1976).

Archean to Proterozoic rocks in the Elliot Lake area

The Archean basement of the southern Wawa-Abitibi Terrane comprises Algoman granitoid rocks and mafic dikes, pillow lavas, and pyroclastic and sedimentary rocks (Frarey 1978) (Fig. 1A).

The Paleoproterozoic Huronian Supergroup is part of the Canadian Shield and overlies the Archean basement, covering an area of ~ 340 km E-W and ~ 300 km N-S (Yamaguchi and Ohmoto 2006) (Fig. 1B). Detailed geological settings of the Huronian Supergroup can be found in Bennett et al. (1991) and Young (1991). The Supergroup is dated

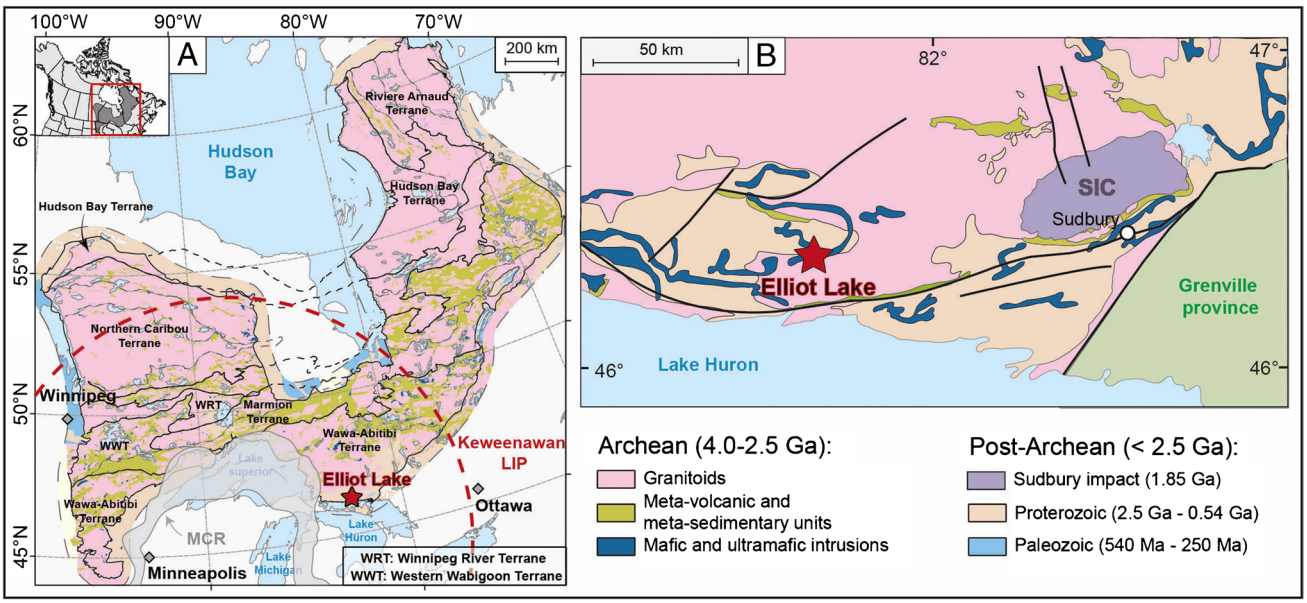

Fig. 1 Regional geologic maps of the study area. **A** Main geologic formations and structures from the Superior Craton (East Canada). The map is after Montsion et al. (2018). Our case study is located in the Wawa-Abitibi terrane, in the SE part of the Superior craton. Keweenawan LIP spatial range and MCR are after Wu et al. (2017) and Stein et al. (2018) respectively. MCR = Midcontinent Rift, LIP = large igneous province; **B** local geological map of the Elliot Lake area, north of Lake Huron and west from Sudbury (Ontario, Canada; after Lightfoot (2017)). Both gold and uranium paleo placers are disseminated within the Proterozoic sediments surrounding Elliot Lake while the Nipissing intrusions are part of the Archean mafic intrusions

between ~ 2450 Ma (age of the underlying Thessalon Formation) and ~ 2217 Ma (age of the cross-cutting Nipissing intrusions) (Bekker and Kaufman 2007) and is composed of four sedimentary units: the Elliot Lake, Hough Lake, Quirke Lake, and Cobalt Groups. These groups were deposited along the Archean cratonic margin during Paleoproterozoic crustal extension (Rousell et al. 2002). The Elliot Lake group is the oldest Huronian unit and consists of the East Bull Lake tholeiitic intrusions, Nipissing Diabase, and Sudbury Gabbro intrusions (Lightfoot 2017).

The Huronian Supergroup and associated intrusive rocks were formed at the southern-rifted margin of the Superior craton, above the far-field Matachewan mantle plume (Lightfoot 2017). In the Elliot Lake area, the Huronian rocks were subjected to low-grade metamorphism of sub-greenschist- to lower greenschist-facies (Easton and Thurston 1992) coevally to the 1850 Ma Sudbury event (Lightfoot 2017). The peak metamorphism is associated with the 1.7–1.9 Ga Penokean Orogeny, which resulted in major shortening and thrusting (Hoffman et al. 1989; Bennett et al. 1991) as well as metasomatism (Fedo et al. 1995; Ulrich et al. 2011).

Current knowledge on mineral resources from the Elliot Lake area

Volcanic and clastic sediments of the Elliot Lake area are associated with economic resources in uranium and minor gold (Robertson 1976; Bergen and Fayek 2012), while the Nippissing diabase (dolerite) dykes contain economic occurrences of Ni-Cu-PGE (Lightfoot 2017).

Anomalous gold values were reported throughout the basin and specifically in the eastern Cobalt Embayment, where paleoplacer gold deposits are found (Roscoe 1976; Mossman and Harron 1983; Long 1986). While the gold-mineralized pyrite grains are detrital (paleoplacer), the ultimate origin of the gold is associated with an Archean source formed between 2.9 and 2.6 Ga, with a peak at 2.7 Ga (Long et al. 2011) located approximatively 1 to 8 km north of the placer (Ulrich et al. 2011).

Ni-Cu-PGE sulfide-rich intrusives are found around the Elliot Lake area such as the Nipissing gabbroic intrusions (2.2 Ga). The style and type of mineralization of these intrusions vary, with variable amounts of Cu, Ni, Co, and PGE over an area of several hundred km at the southern margin of the Superior craton (Sproule et al. 2007). The close proximity of the Elliot Lake area to the Superior craton margin may contribute to a higher fertility in this resource (Griffin et al. 2013).

Uranium-bearing conglomerates are found mainly within the Matinenda Formation, the oldest formation of the Elliot Lake Group, comprising uraniferous quartz–pebble conglomerates. Uraninite grains from these sediments yield U–Pb discordia ages of ~ 1.8 Ga, overlapping the age of the peak metamorphism of the Huronian basin (Ono and Fayek 2011). The Elliot Lake uranium ore deposition model shares the same features as the Witwatersrand world-class paleoplacer deposit located in South Africa (Yamaguchi and Ohmoto 2006; Ono and Fayek 2011; Bergen and Fayek 2012). During extraction of the uranium ore product, HREE and Y in monazites, uraninite and brannerite were collected as a by-product (Castor 2008).

The Midcontinent Rift event (1.1 Ga)

From 1115 to 1085 Ma, the failed north American Midcontinent Rift system (MCR), also called the Keweenawan rift, was initiated contemporaneously with the Grenville orogeny. The MCR affected a 2000 km zone across North America (USA and Canada), including large parts of the southern Superior Craton, located in Canada (Fig. 1; Stein et al. 2011). S-wave tomography measurements reveal that the Elliot Lake area and surroundings were deeply affected by the MCR. An imprint of the rifting event is evidenced by reduced S-wave speeds at depths up to 150 km (Schaeffer and Lebedev 2014) contrasting with the faster S-wave speeds of the surrounding Superior craton. The cratonic root is estimated to be ~ 200 km thick (Darbyshire et al. 2007). The lithospheric disturbance induced from the MCR extends as far north as the Attawapiskat kimberlite field (Hudson Bay, northern Ontario), where Smit et al. (2014) found Mesoproterozoic overprinting/replacement of the lithospheric mantle. The MCR event represents a major heating episode triggered by partial lithosphere removal (Edwards and Blackburn 2018) and generated a large volume of igneous rocks in its southern extent (Nicholson and Shirey 1990). The Lake Superior region, located ~ 100 km NW of the Elliot Lake area, is a major area of exposure of the MCR and shows the widest variety of ore deposit types related to magmatic-hydrothermal activity (Norman 1978).

MCR stages of magmatism and ore deposits

Ore deposits formed in relation to the MCR event are divided into two categories: magmatic and hydrothermal systems (Nicholson et al. 1992). Hydrothermal ore systems in the Superior area include native Cu and Ag in basalts, stratabound copper sulfides and veins, and polymetallic veins (Fe, Cu, Zn, As, Ag, Pb). All hydrothermal mineralization was emplaced 30 to 40 Ma after the main MCR magmatism (Miller et al. 2013). The magmatic ore deposits are Ni-Cu-PGE deposits, Ti-Fe(-V) oxide deposits, sulfide-rich breccia pipes, and Nb-U-REE deposits. The most famous ore deposit from the area is the Keweenaw peninsula native copper district which hosts the largest resource of native Cu in the world (Bornhorst and Mathur 2017).

The MCR magmatism is divided into four stages (Heaman et al. 2007). The first stage (1150–1115 Ma) is associated with basalts and ultramafic dykes, including the 600 km long Abitibi dyke swarm (Wyman and Kerrich 1993), together with minor felsic volcanic rocks. Some of the ultramafic dykes formed at the end of this stage are associated with Ni-Cu-PGE mineralization such as those of the Seagull intrusions (Smyk and Franklin 2007). Stage 2 (1115–1105 Ma) and stage 3 (1100–1094 Ma) are associated with ultramafic and mafic intrusions as well as alkali complexes and bimodal volcanism. These two stages represent the major lithospheric thinning period of the rifting event. Ni-Cu-PGE and Ti-Fe(-V) magmatic deposits are linked to basaltic magmas formed beneath a thin lithosphere lid during this period, including the Duluth complex in Minnesota, USA (Nicholson et al. 1992). Carbonatite-alkali complexes formed beneath regions of thicker lithosphere during these two stages host significant Nb-U-REE resources in apatite and pyrochlore. These deposits are mostly located north of Lake Superior and include the Coldwell, Firesand River and Killala Lake alkali complexes, and the Prairie Lake carbonatites (Nicholson et al. 1992). Stage 4 MCR magmatism (1094–1085 Ma) is associated with late mafic intrusions and porphyries during the thermal collapse of the plume. This stage marks the transition between the magmatic deposits and the beginning of the hydrothermal alteration and leaching which led to secondary metal deposits and mineralized veins (Miller et al. 2013).

Sample petrography

The peridotite xenoliths from Elliot Lake are hosted in a lamprophyre dyke (Fig. 2) that intrudes the Elliot Lake Huronian metasedimentary cover. Twenty peridotite xenoliths of variable size (1–5 cm) were selected for petrography and mineral chemistry, while eight provided enough material for whole-rock analyses.

All peridotites have a similar mineralogy, including olivine (Ol), clino- (Cpx) and ortho-pyroxenes (Opx), and spinel (Sp) as the main phases. They are medium to coarse grained with porphyroclastic orthopyroxenes (up to several mm) and equigranular microstructures for the other minerals (100–300 µm). Based on point-counted mineral mode estimates (Ol: 46–75%, Opx: 24–50%, Cpx: 0.2–2.6%, Sp: 0.2–2.0%), the majority of the studied mantle xenoliths are classified as spinel lherzolites (ESM_1). One sample (sample 4) with only 46% olivine classifies as an olivine websterite. For all samples, the constituent minerals show very little alteration or evidence of mineral, or melt inclusions (a few fluid inclusions are observable in some samples). Intragranular serpentinite and oxides, fractures, and minimal alteration rims surrounding pyroxenes are the only petrographic evidence of secondary processes (Fig. 2). These zones were avoided during ablation analyses. Reaction rims are observed at the interface between xenoliths and their lamprophyre host. These rims are mainly composed of biotite and were excluded from xenolith and lamprophyre powders.

Analytical methods

The peridotite xenoliths are sporadically distributed and small (1–5 cm), limiting opportunities for whole-rock analyses. Among the 20 xenolith sections prepared for mineral chemistry, 8 were suitable to be crushed into powders. The analytical methods are summarized in this section and a detailed version is available in ESM_2.

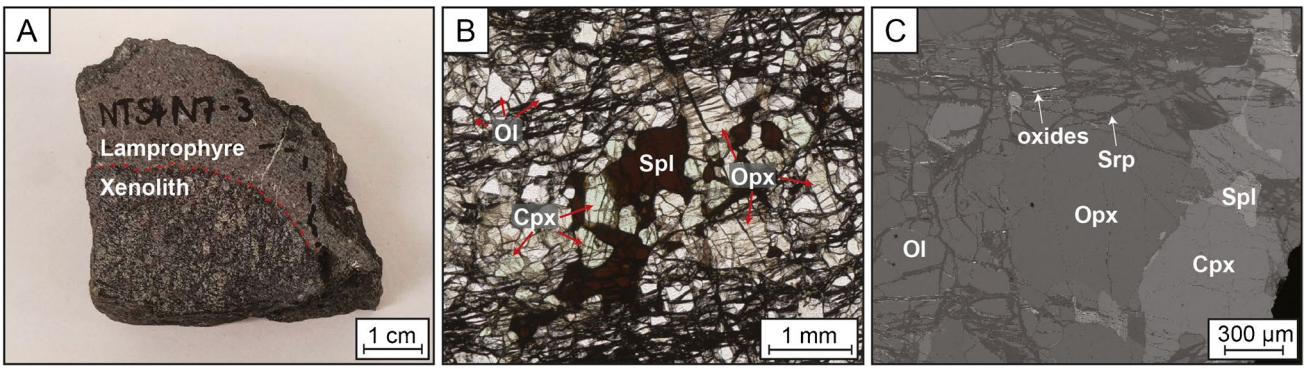

Fig. 2 Representative pictures of the Elliot Lake samples. **A** Macroscopic view of an ultramafic xenolith hosted in a lamprophyre (example of sample 3); **B** microscopic picture of a mantle xenolith from Elliot Lake, in natural light (example of sample 2f). For all samples, main minerals include olivine, orthopyroxene, clinopyroxene and spinel; **C** BSE image taken by the EMPA, showing little alteration of the main mineral assemblage of the xenoliths and very few oxide inclusions within the serpentine alteration (example of sample 2b). Mineral abbreviations are after IMA-approved list. Cpx, clinopyroxene; Ol, olivine; Opx, orthopyroxene; Spl, spinel; Srp, serpentine

Mineral chemistry

In addition to the major mineralogy (ol + cpx + opx + sp), alteration appears as serpentinite and accessory mineral phases such as sulfides have been identified under reflected light and, with a Leica DM 2500 P microscope and with a Zeiss EVO SEM with a LaB6 electron source at the University of Alberta, Canada.

Major elements

Major element mineral analysis was performed at the University of Alberta using a CAMECA SX100 or a JEOL 8900R electron microprobe, on thin sections. Wavelength dispersive spectroscopy (WDS) was employed, at an accelerating voltage of 20 kV, a beam current of 20 nA, and beam diameter of 3 microns. A variety of natural minerals (silicate and oxide) was used for standardization. Data reduction was performed using a ZAF correction along with lower limit of detection filters following the method of Potts (2012). All data including concentrations, limit of detections, and standards are available as ESM_3.

Trace elements

Trace element concentrations in olivine, orthopyroxene, and clinopyroxene were determined by LA-ICP-MS at the University of Alberta, using a RESOnetics Resolution LR50 193 nm laser coupled to a ThermoScientific Element 2XR ICP-MS. Spots were ablated at 13 Hz repetition for 60 s with laser energy of 120 mJ at 11.4% attenuation. For each mineral, 130, 193, or 285 µm spot sizes were chosen to optimize signal according to the space available on the grains. Concentrations were calculated with reference to the NIST612 glass standard and a secondary standard (San Carlos olivine megacryst SC-GB (Bussweiler et al. 2019)), using the Iolite data reduction program ((Paton et al. 2011); https://iolite-software.com/). For internal standardization, olivine, orthopyroxene, and clinopyroxene trace element concentrations are normalized to Si. All data including concentrations, limit of detections, and standards are available as ESM_4.

Whole-rock analyses

Major elements

Whole-rock major element compositions as well as loss-on-ignition (LOI) values were measured using X-ray fluorescence (XRF) at Franklin & Marshall College, United States, on ~2.5 g aliquots of homogenized sample powders following the protocols outlined in Waterton et al. (2020). In addition, analysis of the international reference material harzburgite MUH-1 shows that analytical precision and accuracy for major elements were both typically better than 5%. All sample, standard results, and internal accuracy tests are available in Table 1 and as ESM_5.

Trace elements

Whole-rock trace element compositions of eight peridotite xenoliths and the lamprophyre host were determined by sector-field inductively-coupled plasma mass spectrometry (SF-ICP-MS) at the Arctic Resources Geochemistry Laboratory (ARGL), University of Alberta, using a method modified from Ottley et al. (2003). The analyses were completed on a Thermo Scientific Element XR coupled with an ESI PC3 (a Peltier cooled spray chamber), using an ESI Teflon nebulizer with an uptake rate of approximatively 50 µl/min.

Sample and standard powders were dissolved in acids and doped with 10 ppb In as an internal standard. The element XR is tuned to give a signal sensitivity equivalent to 1.2 MCPS on ^{115}In (1 ppb) and oxide formation rate of around 3% (UO^+/U^+). The auxiliary gas was 0.78 ml/min and the sample gas 1.012 l/min. International reference materials MUH-1 and OKUM were analyzed as secondary standards, and accuracy is generally within 10% or better. The data was processed using an in-house data reduction spreadsheet (Waterton et al. 2017). All sample, standard, and blank results are available in Table 2 and as ESM_5.

Highly siderophile elements

Highly siderophile element (HSE) abundances and Re-Os isotopic compositions were determined at the University of Alberta using isotope dilution techniques modified after Pearson and Woodland (2000). Approximately 1 g of whole-rock powder of the mantle xenolith or the lamprophyre host along with a mixed HSE spike (^{99}Ru, ^{106}Pd, ^{185}Re, ^{190}Os, ^{191}Ir and ^{194}Pt) were dissolved.

Osmium was measured on a Thermo Triton Plus N-TIMS using the axial SEM in a peak-hopping mode. Osmium isotope compositions are corrected for mass-dependent isotope fractionation and oxygen isotope interferences. SEM yield and performance were monitored using 0.5 ng loads of a Durham Osmium Standard (DROsS; $^{187}Os/^{188}Os = 0.160746 \pm 0.000074$; 2σ; $n = 7$) that yielded results in agreement with the original determination of the DROsS value by N-TIMS on 10–100 ng aliquots (0.160924 ± 0.000004; 2σ; (Luguet et al. 2008)).

The other HSEs were measured on a Thermo Element XR2 ICP-MS using a Peltier-cooled micro-concentric nebulizer. Solutions of 1 ppb in-house standards for each target element were analyzed to measure and correct for instrumental mass bias. The accuracy of the chemistry was verified using one blank and one standard (OKUM) as summarized in detail in Waterton et al. (2021).

Table 1 Whole-rock major element and HFSE composition of the xenoliths and lamprophyre from Elliot Lake

Sample	1a	1b	2a	2b	3	4	6b	6d	Lamprophyre
Major elements (wt.%)									
SiO_2	42.43	44.94	44.51	42.98	43.95	45.24	42.92	43.11	40.21
TiO_2	0.01	0.00	0.09	0.23	0.10	0.06	0.10	0.35	1.03
Al_2O_3	1.24	1.65	2.62	2.98	2.42	2.13	1.73	4.12	8.56
Fe_2O_{3T}	9.36	8.47	8.51	9.18	8.48	8.59	10.46	9.16	10.25
MnO	0.09	0.09	0.10	0.12	0.12	0.10	0.12	0.13	0.17
MgO	44.83	43.09	40.22	38.89	40.03	39.89	41.36	34.44	21.29
CaO	1.00	1.26	2.53	3.74	3.36	3.00	1.98	6.40	14.30
Na_2O	0.09	0.08	0.11	0.12	0.17	0.14	0.17	0.20	0.55
K_2O	0.06	0.02	0.34	0.80	0.41	0.26	0.40	1.24	3.22
P_2O_5	0.01	0.01	0.05	0.14	0.11	0.05	0.05	0.21	0.51
Total	99.13	99.61	99.08	99.18	99.15	99.46	99.29	99.35	100.08
LOI	7.80	7.91	7.52	6.16	5.75	8.11	5.56	7.13	6.10
Mg #	0.89	0.90	0.89	0.88	0.89	0.89	0.87	0.87	0.78
Cr (ppm)	2233	2547	3353	2317	2790	2180	1651	2378	1479
PGE (ppb)									
Os	1.12	1.28	2.05	6.81	13.61	1.78	2.34	0.64	0.26
Ir	1.15	0.58	1.04	1.67	3.82	1.46	1.90	0.89	0.41
Pt	3.37	1.90	1.16	1.98	2.31	5.46	2.48	1.88	4.14
Pd	1.89	0.48	0.51	0.98	0.68	0.36	1.24	0.98	2.87
Re	1.60	0.35	2.57	0.25	0.42	0.44	0.45	0.52	0.99
Re^{187}/Os^{188}	6.89	1.32	6.05	0.18	0.15	1.20	0.93	4.08	18.53
Abs. 2σ	*0.67*	*0.05*	*0.20*	*0.01*	*0.01*	*0.05*	*0.03*	*0.20*	*0.57*
Os^{187}/Os^{188}	0.13	0.12	0.12	0.12	0.12	0.12	0.12	0.15	0.24
Abs. 2σ	*0.0002*	*0.0002*	*0.0002*	*0.0002*	*0.0002*	*0.0002*	*0.0002*	*0.0002*	*0.0003*
T_{RD} (Ma)	Neg	781	1077	1028	1402	483	971	Neg	-
$T_{RDErupt}$ (Ma)	-	-	-	1485	1788	3574	3345	-	-
T_{MA} (Ma)	11.5	Neg	Neg	1750	2155	Neg	Neg	280	-

Table 2 Whole-rock trace element composition of the xenoliths and lamprophyre from Elliot Lake

Sample	1a	1b	2a	2b	3	4	6b	6d	Lamprophyre
Trace elements (ppm									
Sc	0.84	1.1	0.59	1.5	0.21	1.3	0.26	0.03	3.6
Ti	9.4	1.8	64	147	39	42	62	190	775
V	3.2	4.4	6.1	7.0	4.5	5.7	4.0	7.5	20
Co	11	11	9.9	9.9	8.6	9.8	11	8.6	8.4
Ni	221	210	185	178	166	185	181	139	76
Cu	0.53	0.35	0.89	1.4	0.68	0.63	0.75	1.9	6.0
Ga	0.09	0.09	0.20	0.26	0.12	0.14	0.15	0.32	1.1
Zr	0.24	0.01	1.4	3.4	0.80	0.99	1.5	4.3	41
Rb	0.23	0.10	1.21	2.5	1.3	1.0	1.4	4.0	13
Sr	2.0	0.57	9.7	23	17	13	13	40	131
Y	0.05	0.03	0.16	0.42	0.13	0.14	0.12	0.43	1.8
Nb	0.13	0.01	0.69	2.0	0.44	0.55	0.70	2.0	8.6
Mo	1.4	0.55	0.39	0.59	0.46	0.70	0.66	0.72	0.35
Cs	0.11	0.09	0.26	0.33	0.36	0.45	0.47	0.56	7.1
Ba	2.7	0.15	21	48	12	14	17	63	277
La	0.18	0.05	0.67	1.7	0.54	0.54	0.55	1.9	6.9
Ce	0.33	0.08	1.4	3.9	1.3	1.2	1.2	4.5	15
Pr	0.04	0.01	0.17	0.45	0.19	0.15	0.14	0.53	1.8
Nd	0.15	0.02	0.69	1.8	0.78	0.60	0.58	2.2	7.1
Sm	0.02	0.00	0.11	0.29	0.12	0.09	0.09	0.35	1.2
U	1.7	0.85	0.21	0.70	0.38	0.32	0.24	0.90	0.11
Trace elements (ppb)									
Eu	73	17	338	820	331	278	284	1031	3485
Gd	198	27	853	2300	889	733	744	2744	9596
Tb	21	4	89	241	87	76	76	284	974
Dy	97	30	365	975	319	306	304	1099	3787
Ho	18	9	64	166	53	54	50	181	620
Er	54	38	173	428	140	147	123	450	1518
Yb	62	61	176	374	134	146	106	385	1264
Lu	11	12	28	57	21	24	17	57	203
Hf	47		273	677	163	215	404	929	9279
Ta	50	3	319	880	217	234	346	982	3653
Pb	340	199	995	1789	865	823	926	2613	6186
Th	102	14	323	1190	127	323	278	794	3932

Table 3 Rb–Sr isotopic measurements from mica fractions from the Elliot Lake lamprophyre host

					Normal isochron				*Inverse isochron*					
Sample Name	*Fraction*	*Weight (mg)*	*Sr (ppm)*[1]	*Rb (ppm)*[1]	$^{87}Rb/^{86}Sr$	*Rb_prop_er (2σ, abs)*	$^{87}Sr/^{86}Sr$	*Sr_prop_er (2σ, abs)*	$^{87}Rb/^{87}Sr$	*Rb_prop_er (2σ, abs)*	$^{86}Sr/^{87}Sr$	*Sr_prop_er (2σ, abs)*	*T (Ma)*	*T_er (2σ, abs)*
HL-1	Mica	3.9	193	280	4.24	0.032	0.770273	0.000009	5.50	0.041	1.2982	0.00002	1088	8.16
HL-2	Mica	3.8	193	280	4.22	0.032	0.770394	0.000009	5.48	0.041	1.2980	0.00002	1094	8.21
HL-3	Mica	3.5	244	349	4.16	0.031	0.769533	0.000010	5.40	0.041	1.2995	0.00002	1096	8.23
HL-4	Mica	6.6	193	274	4.13	0.031	0.769122	0.000010	5.37	0.040	1.3002	0.00002	1096	8.23
HL-5	Mica	5.8	206	298	4.21	0.032	0.770194	0.000010	5.47	0.041	1.2984	0.00002	1094	8.21
HL-6	Mica	4.5	199	279	4.08	0.031	0.768355	0.000011	5.31	0.040	1.3015	0.00002	1096	8.23
HL-7	Mica	5.0	248	346	4.06	0.030	0.768110	0.000008	5.28	0.040	1.3019	0.00001	1099	8.25
HL-8	Leachate	5.8	715	255	1.03	0.008	0.720428	0.000009	1.43	0.011	1.3881	0.00002	1093	8.20

prop_er propagated error, abs absolute

[1]concentration errors are at ca. 10%

Lamprophyre Rb–Sr mica dating

Samples of the lamprophyre host were processed at the Arctic Resources Laboratory (University of Alberta) via electrical fragmentation with a SELFRAG Lab System. Seven fractions of mica grains of 3.5 to 6.6 mg were handpicked for Rb–Sr column chemistry. The batch was accompanied by one leachate, two standards (BHVO-2), and a blank. Each phlogopite fraction was spiked with a mixed ^{87}Rb-^{84}Sr spike. Rb was analyzed in a 10% HNO_3-2% HF-5 ppb Zr solution, using a Thermo ICAP-Q quadrupole inductively coupled plasma mass spectrometer. Sr was analyzed using a Thermo Triton Plus Multicollector Thermal Ionization Mass Spectrometer, loaded with TaF_6 onto Re filaments. 10 to 1 ng SRM987 Sr standards were loaded alongside unknown samples. Model ages are calculated using initial $^{87}Sr/^{86}Sr$ of 0.7035, 0.705, and 0.710. Isochron plots and isochron calculated ages are produced using IsoplotR (Vermeesch 2018). USGS international reference material NBS 987 yields a Sr isotope composition within error of its accepted value (0.710265). All data including ratios, errors, and standards are available as Table 3 and ESM_6.

Mineral geochemistry results

Major element composition

Mineral major element compositions of the Elliot Lake xenoliths are reported in ESM_3. Peridotite equilibration pressures and temperatures at the time of lamprophyre

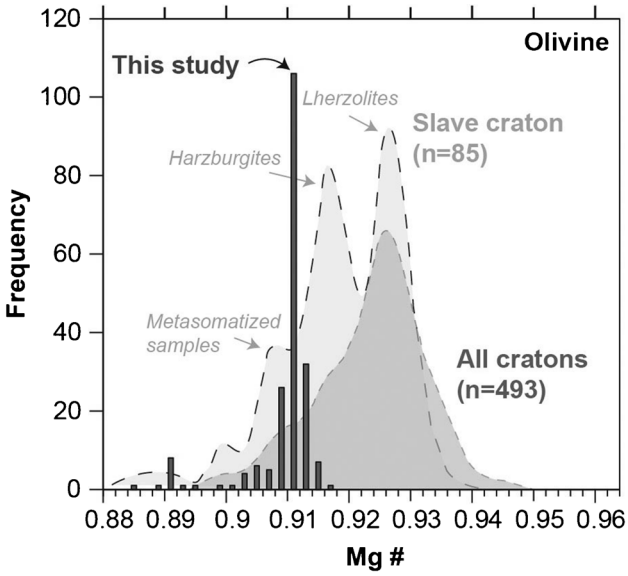

Fig. 3 Histogram of olivine Mg# compared to the range of olivine Mg# in the Slave craton and average cratonic settings worldwide (Pearson and Wittig 2014)

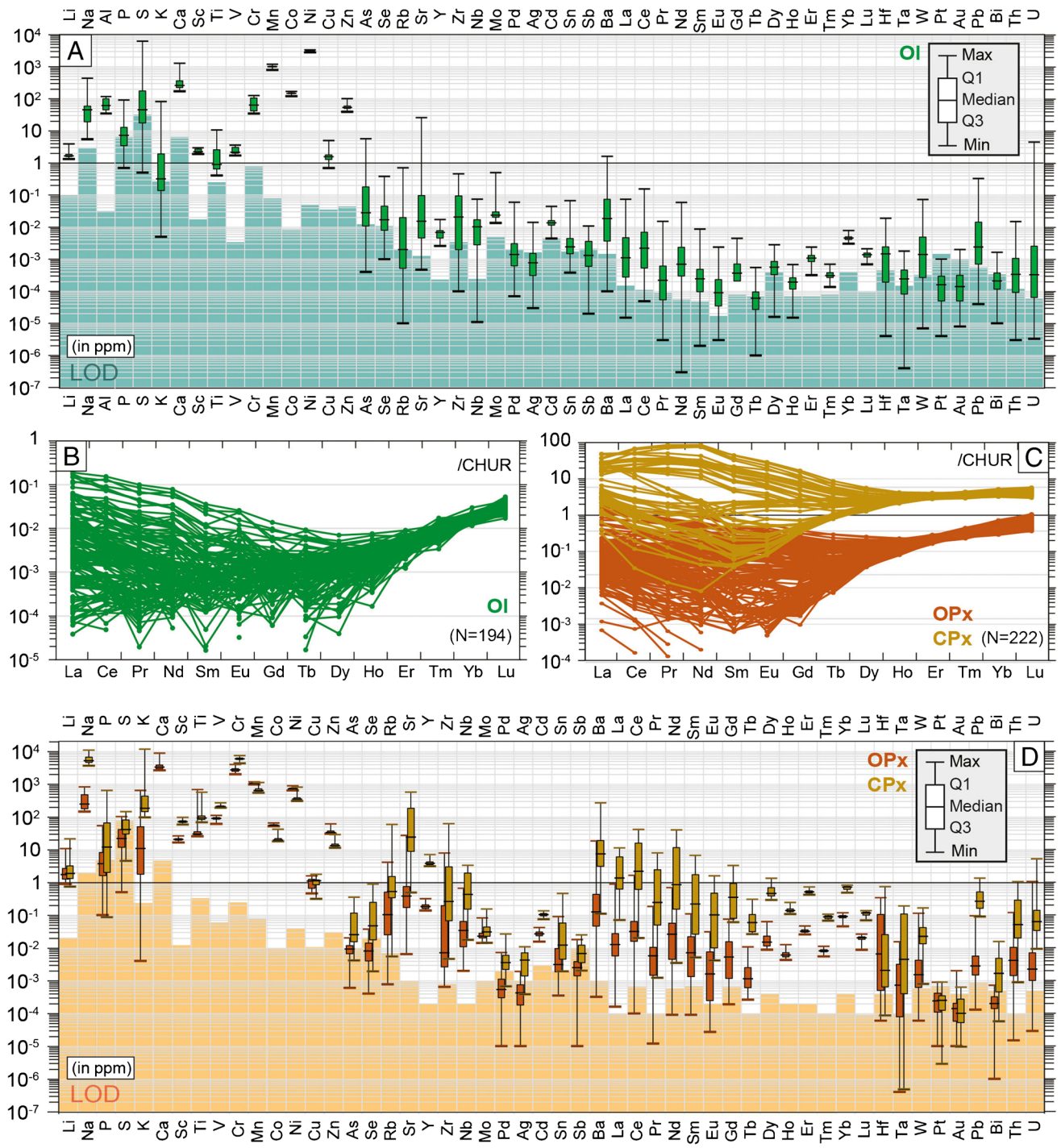

Fig. 4 Trace element composition of olivine, orthopyroxene and clinopyroxene from Elliot Lake xenoliths. **A – B** Trace element data and REE patterns (normalized to CHUR; McDonough and Sun (1995)) of olivine analyses; **C – D** measurements in orthopyroxenes and clinopyroxenes. All data from A and D are displayed as box plots with the minimum value, first quartile (25%), median, third quartile (75%), and maximum value; the limit of detection (LOD) is shown as a shaded area (average of all LOD for each element). All analyses are in ESM_4

eruption were calculated using the major element data in the PTEXL spreadsheet (Stachel 2022). Calculations are detailed in the discussion section of the manuscript.

Olivine Mg# ranges between 0.88 and 0.91, with more than 75% of olivine clustering around 0.91 (Fig. 3). The Elliot Lake xenoliths are part of the Superior craton, but

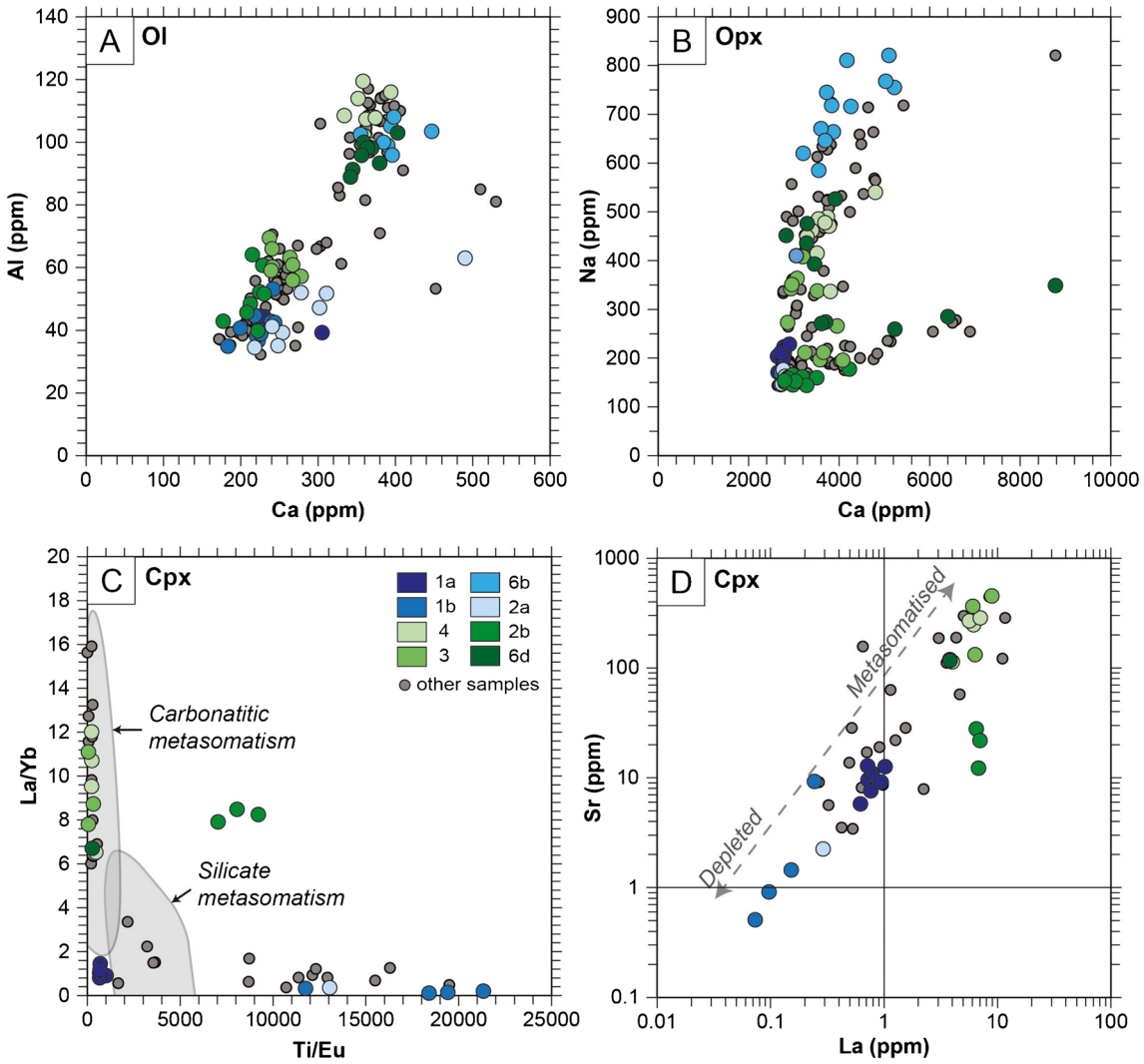

Fig. 5 Trace element biplot diagrams from **A** olivine, **B** orthopyroxene, and **C–D** clinopyroxene analyses from the Elliot Lake xenoliths. Carbonatitic and silicate metasomatism domains are after Coltorti et al. (1999). Metasomatised and depleted area of Sr-La diagram are after Tang et al. (2008). Cpx, clinopyroxene; O, olivine; Opx, orthopyroxene. The grey dots represent samples for which whole-rock data could not be acquired

have Mg# lower than typical Archean cratonic peridotites with a mode of ~ 0.93 (Pearson and Wittig 2014).

Orthopyroxene has a mean Mg# of 0.91 similar to olivine. Its high Al_2O_3 (3.0 to 3.8 wt.%) content is consistent with equilibration in the spinel facies. Orthopyroxene Cr_2O_3 ranges from 0.35 to 0.56 wt.% and has low TiO_2 (0.01 to 0.13 wt.%), CaO (0.33 to 0.57 wt.%), and Na_2O (0.02 to 0.09 wt.%) compared to cratonic spinel xenoliths.

All analyzed clinopyroxene are Cr-diopsides, with Mg# values higher than olivine and orthopyroxene, between 0.90 and 0.94. They have low TiO_2 (0.01 to 0.34 wt.%), relatively low Na_2O (0.45 to 1.41 wt.%) and high CaO (18.4 to 22.2 wt.%) compared to cratonic spinel peridotites.

Spinel compositions of our samples are typically between the spinel and magnesiochromite endmembers with high Mg# from 0.70 to 0.76, low Cr# of 0.20 to 0.26, and high Al_2O_3 (45 to 51 wt.%), and variable TiO_2 (0.01 to 0.08 wt.%) compared to cratonic spinel xenoliths.

In situ trace element composition

Among Elliot Lake xenoliths, 18 permitted in situ trace element measurement, which resulted in 148 olivine and 170 orthopyroxene measurements, while 14 peridotites allowed 52 clinopyroxene analyses (ESM_4).

Olivine

Elliot Lake peridotite olivines have significant but widely varying Na, Al, Co, and Zn concentrations and ppm levels for Li, P, S, Sc, Ti, V, and Cu, while the other measured elements are mostly at the ppb level. Concentrations of Pd, Ag, Pt, and Au are mostly below the limit of detection (Fig. 4), as also found for Slave peridotite olivine by Veglio et al. (2022).

Based on Na, Al, P, Ca, Sc, Ti, V, Cr, Zn, Y, Zr, and Ta concentrations in olivine samples can be separated into two distinct groups (Fig. 5A). Those with low Ca concentrations (below 300 ppm) show a positive correlation between Na, Al, Ca, Ti, V, Cr, and Y. The group with high Ca concentrations commonly does not display any internal correlation between elements despite significant variability but follows the Na, Al, Ca, Ti, V, Cr, and Y correlations of the first group. Samples with the highest bulk rock Al and Ca concentrations do not necessarily have the highest Al and Ca content in olivine. Chondrite-normalized REE patterns have highly variable LREE values that reflect varying levels of metasomatism, whereas the HREE are negatively sloped and in the expected range for spinel lherzolites (Pearson et al. 2014).

Orthopyroxenes

Elliot Lake peridotite orthopyroxenes have ppm level concentrations of Li, P, K, Sc, Ti, V, Co, Cu, and Zn, while other measured elements are mostly at the ppb level except Pd, Ag, Sb, Pt, Au, and Bi, which are mostly below the limit of detection (Fig. 4).

Two compositional trends can be distinguished through Na and Ca variation (Fig. 5B). The high Na trend (trend with steep slope) has positive correlation with Ti, Zn, Y, Zr, Nb, Sn, and Ta and a decrease in HREE concentrations. This trend is typically

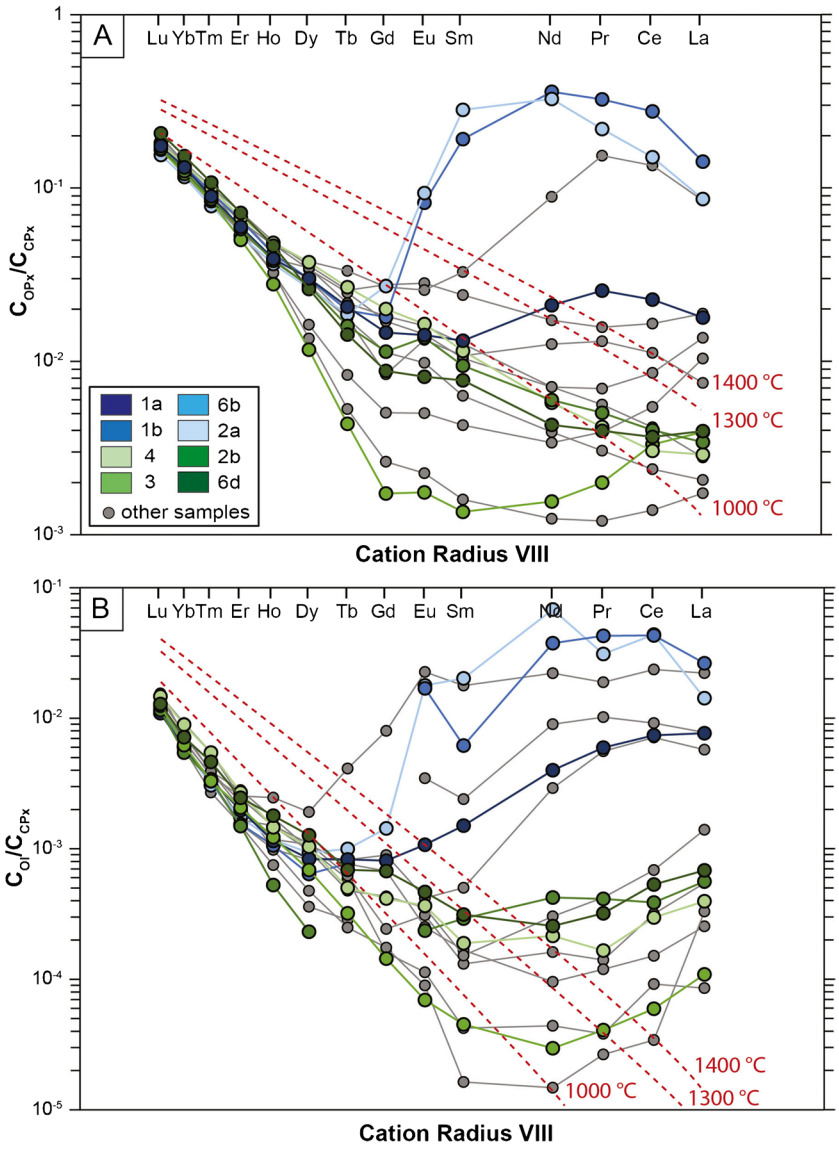

Fig. 6 Partition coefficient between Opx and CPx (**A**) and Ol and CPx (**B**) for each rare earth element. Dashed lines indicate equilibrium between minerals at specific temperatures (Agranier and Lee 2007). The color scheme reflects the degree of depletion/metasomatism as illustrated in Fig. 5D. The grey dots represent samples for which whole-rock data could not be acquired

illustrated by sample 6b. The high Ca trend (trend with gentle slope) is positively correlated with Cr, Y, Sn, and Ta, e.g., sample 2b and 6d. Some elements are present in both trends, but the correlation slope is different. Orthopyroxenes have highly variable LREE concentrations reflecting metasomatism, while the HREE are in the expected range for spinel lherzolites (Fig. 4c) (Scott et al. 2016). Similar to olivine, elemental variation in orthopyroxene does not necessarily reflect variations observed in bulk rock data.

Clinopyroxenes

Elliot Lake peridotite clinopyroxenes have ppm levels of Li, P, K, Sc, V, Co, Cu, Zn, Sr, Y, Ba, and LREE, while other elements are mostly at the ppb level and Pt and Au are mostly below the limit of detection (Fig. 4).

In contrast to olivine and orthopyroxene, clinopyroxene exhibits a distinct separation between samples that show variable depletion in LREE (high Ti/Eu in blue in Fig. 5) and those that have relatively higher concentrations in LREE (low Ti/Eu in green in Fig. 5). The high LREE clinopyroxene has significantly higher La, Sr, and La/Yb (Fig. 5), characteristic of carbonatitic-like metasomatism (Coltorti et al. 1999). This contrasts with the more LREE depleted samples that show greater concentrations in Ti and thus Ti/Eu, which is consistent with kimberlite-type metasomatism (e.g., Shu and Brey (2015)).

Trace element correlation between minerals

Application of the partitioning diagrams between olivine, orthopyroxene, and clinopyroxene designed by Agranier and Lee (2007) shows consistency with equilibrium of the HREE below 1000 °C and significant redistribution of the LREE. LREE are most commonly mobile (Scott et al. 2016) and give a more accurate reflection of the extent of metasomatism, which is significant in our samples (Fig. 6). Among the other elements measured above the limit of detection for each mineral, seven are of potential economic interest and also show correlations at the whole-rock scale Cu, Y, Zr, Nb, Ta, Pb, and U. Overall, most elements show a large spread of measured concentrations (Fig. 4), from 1 to 5 orders of magnitude, which is symptomatic of metasomatism. However, for elements with limited spread like Y, the relative concentration distribution among the three main minerals of the peridotites is as expected from partitioning observations (Eggins et al. 1998).

Whole-rock chemistry results

Major elements

The lamprophyre has an intermediate composition between a calc-alkaline and Mg-rich ultramafic lamprophyre (Rock 1991). The lamprophyre composition shown in Table 1 is the average of four separate analyses of the same sample. All analyses were within uncertainty and show that this composition reflects a homogeneous matrix.

Peridotite whole-rock major element and LOI data are given in Table 1. The mean LOI is 7.3% indicating extensive alteration of the samples, despite the moderate-looking alteration of the samples (Fig. 2). The lack of correlation between LOI values and major oxides suggests that the dominantly

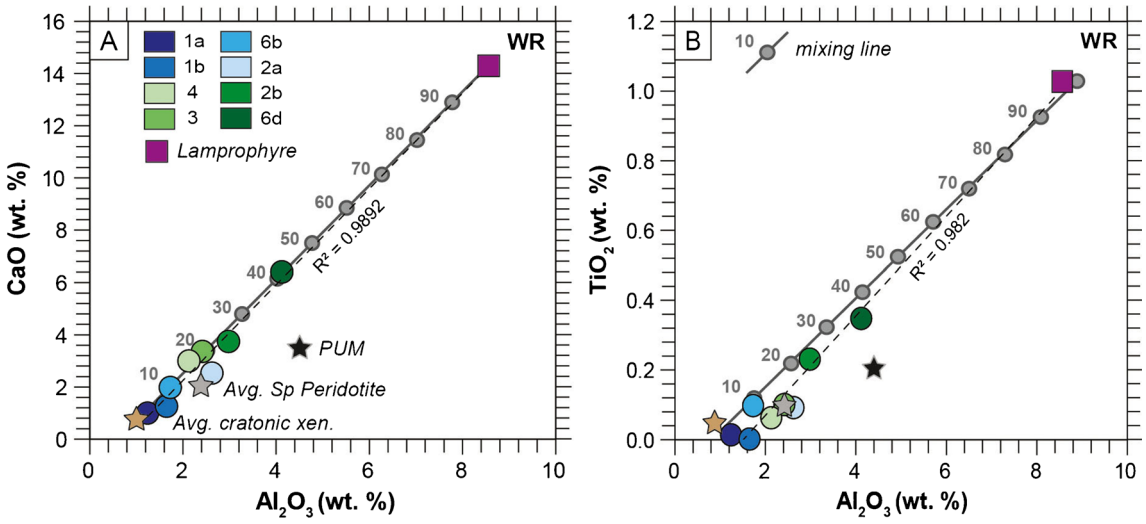

Fig.7 Variations in whole-rock major element composition between xenoliths resulting from melt depletion and refertilisation processes in the upper mantle. Reference values are from Pearson et al. (2014). The color scheme reflects the degree of depletion/metasomatism consistently with Fig. 5D

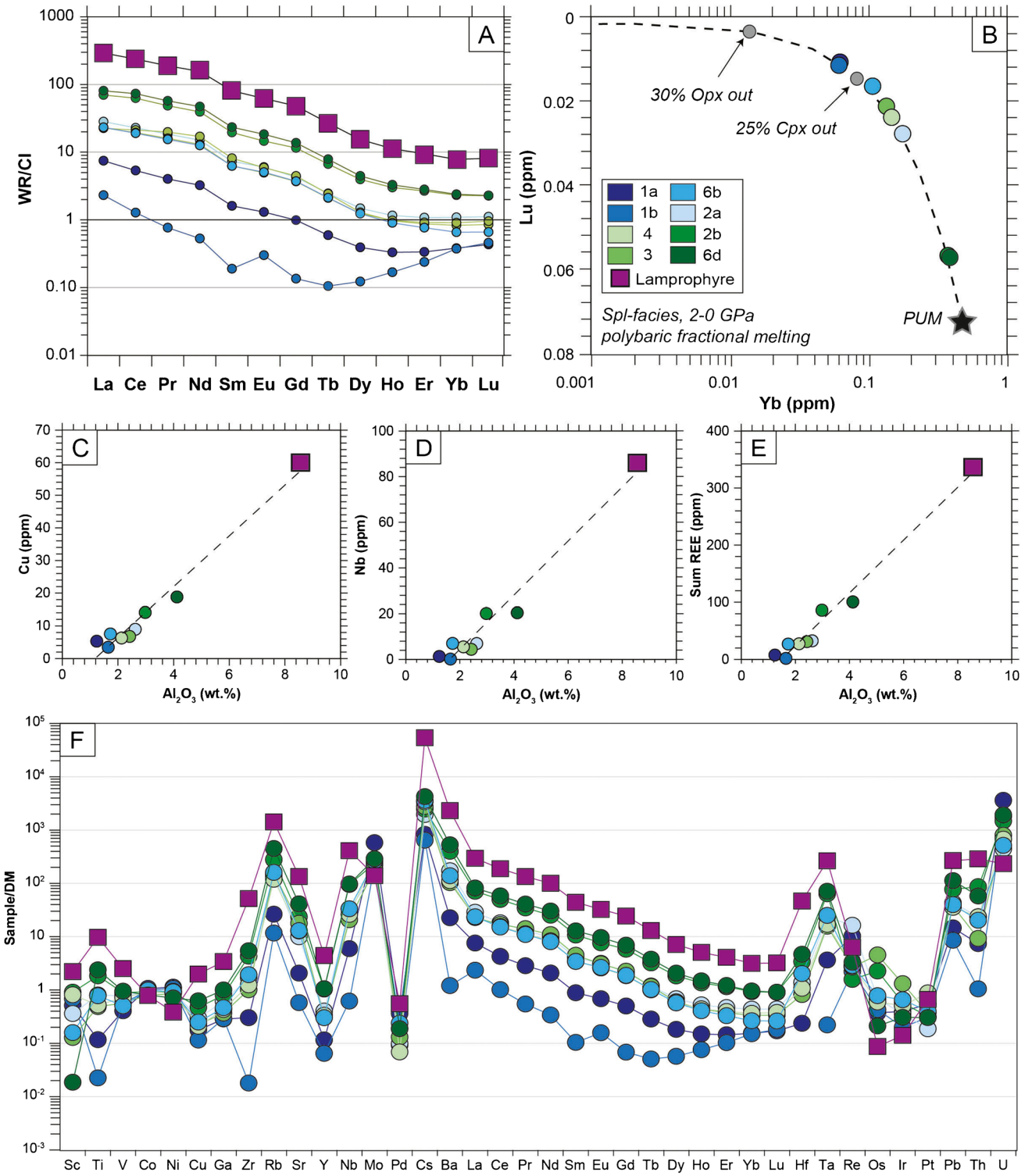

Fig.8 Whole-rock trace element composition of mantle xenoliths and their lamprophyre host rock from Elliot Lake, Canada; **A** Xenolith and lamprophyre REE compositions normalized to CI-chondrite (McDonough and Sun 1995). **B** Yb and Lu systematics of residue evolution at low pressure during mantle melting (Wittig et al. 2008). Primitive mantle (PUM) is after McDonough (1990). **C**, **D**, **E** Covariation of metal content between the studied xenolith suite and the lamprophyre host. **F** Spider diagram of all trace elements measured in the xenoliths and the lamprophyre (normalized to the Depleted mantle). The color scheme reflects the degree of depletion/metasomatism as illustrated in Fig. 5D and Fig. 7

hydrous alteration is not related to sub-surface processes (Boyd et al. 1997) and mainly due to serpentinization of the peridotites.

The peridotites have moderate to high MgO (34–45 wt.%) and high Fe_2O_{3T} (8.5–10.5 wt.%) contents compared to average cratonic peridotites, yielding low whole-rock Mg# of 0.87 to 0.90. Al_2O_3 (1.2 to 4.1 wt.%) shows a strong correlation with CaO (1.0 – 6.4 wt.%), as well as TiO_2 (Fig. 7A, B), ranging from very low values, typical of cratonic peridotites (Pearson and Wittig 2014), to values in excess of estimates for primitive upper mantle (Fig. 7). TiO_2 varies from 0.002 to 0.348 wt.% and is also positively correlated with K_2O (0.02 to 1.24 wt.%) and P_2O_5 (0.006 to 0.205 wt.%). The majority of Elliot Lake peridotites plot along the melt depletion trend described in Liu et al. (2018), ranging from compositions close to refractory cratonic mantle to fertile primitive upper mantle (PUM) (McDonough and Sun 1995; Pearson and Wittig 2014). However, the samples with the highest concentrations extend beyond the fertile mantle, with compositions trending towards the lamprophyre host (Fig. 7). If the xenoliths had an original composition close to the average cratonic peridotite composition, up to ~ 40% mixing with the lamprophyre host would be needed to explain the spread of our samples (Fig. 7), though this value would be much lower if the starting composition was less depleted.

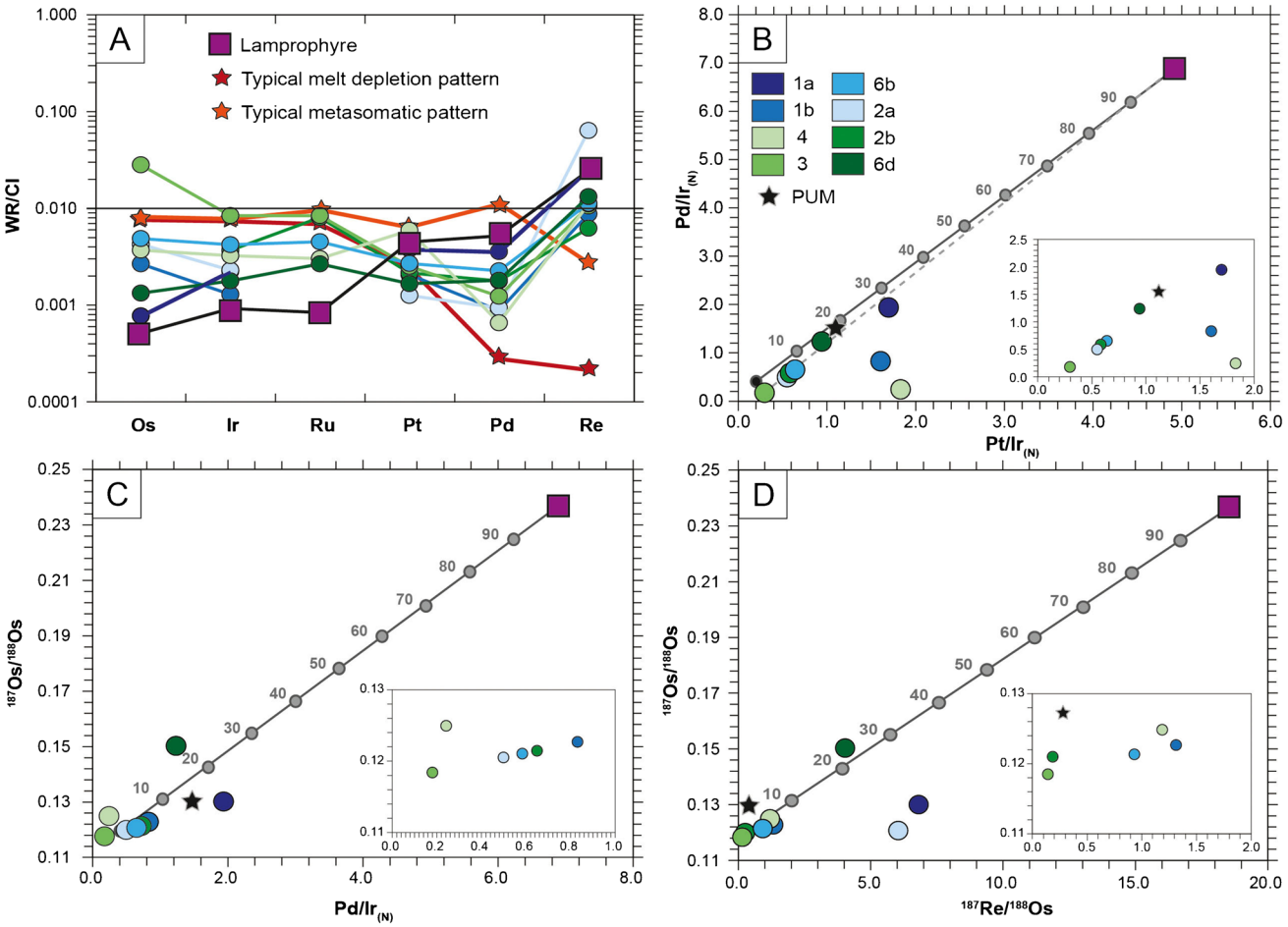

Fig. 9 Whole-rock PGE contents and Re-Os isotopic values for the Elliot Lake xenolith suite and the lamprophyre host. **A** Platinum group element pattern of the mantle xenoliths compared to the lamprophyre host rock. Values are normalized to CI-chondrite (Fischer-Gödde et al. 2011). Typical pattern of melt depletion and metasomatic signature are after the Lesotho data reported by Pearson and Wittig (2014); **B** Covariation of $Pd/Ir_{(N)}$ versus $Pt/Ir_{(N)}$ of mantle xenoliths and the lamprophyre, indicating disturbed PGE systematics; **C** Correlation of $^{187}Os/^{188}Os$ and $Pd/Ir_{(N)}$ values, where the Os isotope values can be used as a proxy for formation age, or indicate metasomatism (radiogenic $^{187}Os/^{188}Os$); **D** Re-Os isotopic ratios for all samples. PUM value as described in Becker et al. (2006). Mixing lines between a typical cratonic xenolith and the lamprophyre host are drawn for B, C and D. Cratonic xenolith composition is set according to Pearson et al. (2004). The color scheme reflects the degree of enrichment as illustrated in Fig. 5

Minor and trace elements

Whole-rock minor and trace element concentrations are given in Table 2. Minor element variability includes Co (86 to 113 ppm), Ni (1390 to 2214 ppm), Sr (6 to 404 ppm), and Ba (1 to 634 ppm), with incompatible Ti, Sr, and Ba being far above the levels expected for melting residues. Trace elements at the ppm level include Sc, V, Cu, Ga, Rb, Y, Zr, Nb, Mo, Cs, U, and LREE. MREE, HREE while Pb and Th are at the ppb level.

All measured elements, except Ni and Co, correlate positively with the whole-rock Al_2O_3 content. As with the major elements, some peridotites show elevated values compared to the proposed values for the primitive upper mantle (PUM) presented in McDonough (1990). Chondrite-normalized whole-rock REE patterns for the xenoliths are characterized by negative sloping LREE-MREE and flat HREE, with LREE concentrations ranging from ~ 1 to 100 times the chondrite value (Fig. 8A). The high REE concentration is similar to that observed for major elements with samples 1a and 1b as the most depleted and samples 2b and 6d as the most elevated values and closest to the lamprophyre concentrations.

As expected, the Elliot Lake lamprophyre is characterized by elevated incompatible minor and trace element concentrations compared to the peridotite xenolith it carries (Fig. 8F), except for Co, Ni, Mo, and U which are more depleted. A linear correlation exists between the xenolith and the lamprophyre host for the following elements: Ti, V, Cu, Ga, Rb, Sr, Y, Zr, Nb, Cs, Ba, Hf, Ta, Pb, Th, and REE (e.g., Fig. 8C, D, and E). This line could represent a mixing line.

HSE chemistry

Highly siderophile element concentrations for the peridotite xenoliths and the lamprophyre are summarized in Table 1. The HSE systematics of the Elliot Lake peridotites are complex. Osmium and Ir concentrations are generally lower than PUM (Becker et al. 2006), ranging from 0.64 to 2.3 ppb and 0.6 to 1.9 ppb, respectively. Only peridotites 3 and 2b fall outside this range, with PUM-like Ir abundances (3.8 ppb) and elevated Os (13.6 and 6.81 ppb). Chondrite-normalized (CI-chondrite; Fischer-Gödde et al. 2011) HSE patterns are overall flat with a minor negative Pd anomaly (0.48–1.9 ppb) and elevated Re concentrations above the PUM value (0.25–2.6 ppb) (Fig. 9A). Elliot Lake samples have sub- to supra-chondritic Pd/Ir ratios ($Pd/Ir_{(N)}$ = 0.2 to 2.0), Pt/Ir ratios ($Pt/Ir_{(N)}$ = 0.3 to 1.9), and Os/Ir ratios ($Os/Ir_{(N)}$ = 0.2 to 3.3). There are no clear correlations between major element and HSE concentrations or ratios. However, the two xenoliths with extreme Al_2O_3 values exhibit the highest Pd/Ir ratios (1a and 6d). Most samples have a clear positive correlation between the $Pd/Ir_{(N)}$ and $Pt/Ir_{(N)}$ ratios except for samples 1b and 4 (Fig. 9B).

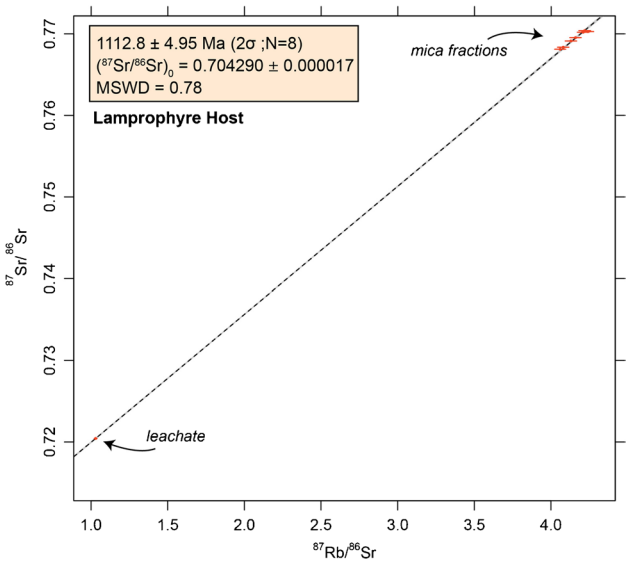

Fig. 10 Isochron calculated from the mica fractions extracted from the lamprophyre host erupted at Elliot Lake. Error is at 2σ level. Unanchored result (without leachate) is 952.4 ± 167 Ma (2σ, MSWD = 0.44)

Re-Os isotopes

Elliot Lake peridotites have a large range of whole-rock $^{187}Os/^{188}Os$ ratios (0.1183–0.1592; Table 1), which can be divided into two groups (Fig. 9C and D): (1) sub-chondritic Os isotope ratios with an average value of 0.12 (1b, 2a, 2b, 3, 4, 6b) and (2) two radiogenic samples at 0.13 (1a) and 0.15 (6d). The radiogenic values correspond to the most elevated (high Al_2O_3 concentration, sample 6d) as well as most depleted (low Al_2O_3 concentration, sample 1a) whole-rock major element analysis. Peridotites with the highest $^{187}Os/^{188}Os$ values show the highest $Pd/Ir_{(N)}$ and lowest $Os/Ir_{(N)}$.

Whole-rock $^{187}Re/^{188}Os$ ratios span a large range (0.1–6.9). All values are above PUM except samples 2b and 3. Three samples have higher $^{187}Re/^{188}Os$ ratios (> 2.0; 2a, 6d, 1a), two of which also having the highest $^{187}Os/^{188}Os$ values.

Elliot Lake peridotites show considerable scatter on the $^{187}Os/^{188}Os$ vs $^{187}Re/^{188}Os$ diagram, with samples extending to very high $^{187}Re/^{188}Os$ ratios (Fig. 9D). The group of peridotites with sub-chondritic $^{187}Os/^{188}Os$ (1b, 2b, 3, 4, 6b) form a scattered array, whose extension to $^{187}Re/^{188}Os$ values that are well above PUM (to ca. 7), indicates that the dispersion is mostly likely due to metasomatism/mixing, rather than melt extraction (Fig. 9D).

Rb–Sr mica dating of the lamprophyre host

Rb–Sr isotopic data were acquired for 7 mica fractions and one leachate from the Elliot Lake host lamprophyre intrusion (Table 3). All mica fractions have similar Sr and Rb concentrations of 190–250 ppm and 275–350 ppm, respectively, and define a tight range of Rb/Sr ratios (1.39 to 1.46). The leachate has a higher Sr concentration of 715 ppm and lower Rb concentration of 254 ppm, providing a lower Rb/Sr anchor on an isochron diagram.

The seven mica fractions define an isochron array with an age of 952.4 ± 167 Ma (2σ, MSWD = 0.44). When the leachate is included, to anchor the regression, the resulting isochron gives an initial $^{87}Sr/^{86}Sr$ of 0.704290 ± 0.000086 and an age of 1112.8 ± 4.95 Ma (2σ, MSWD = 0.79) (Fig. 10), clearly indicating a Midcontinent Rift age for this intrusion, consistently with previous work on magmatism associated with this event (Heaman et al. 2007). The elevated initial ratio at 1.1 Ga indicates that the source region was likely reworked by a prior subduction event.

Discussion

Melt depletion of the Mesoproterozoic southern Superior craton root

Peridotites with olivine compositions of Mg# ca. 91 sampled by the 1.1 Ga Elliot Lake lamprophyre have major element systematics that are, on average, more melt-depleted than estimates of fertile mantle, but are less melt depleted than the peridotites that form the roots beneath the Archean cratonic cores (Fig. 3A; Pearson et al. 2021). The co-linear relationship of the Elliot Lake peridotites between depleted mantle compositions and higher CaO and Al_2O_3 compositions that range from below to beyond PUM (Fig. 7) is indicative of a combination of melt depletion and metasomatic enrichment/modification (O'Reilly and Griffin 2013). The most depleted major element compositions of the Elliot Lake peridotites range between the average "off-craton" spinel peridotite composition of McDonough (1990) and the expected mean cratonic composition (Pearson et al. 2014). Most samples have compositions that are more enriched in SiO_2, CaO, Al_2O_3, K_2O, and TiO_2 than the average Archean cratonic peridotite that we would expect in Elliot Lake (Fig. 7). These more enriched compositions, along with depleted Pd but elevated Re concentrations, reflect metasomatic enrichment of a moderately depleted peridotite protolith (Pearson et al. 2002).

Due to the re-fertilization, it is difficult to evaluate how melt-depleted the peridotite protolith was, but none of the olivine compositions have Mg#s as high as average Archean cratonic mantle (Fig. 3; (Pearson and Wittig 2014)). However, all samples scatter around the ~ 2 to 0 GPa polybaric fractional melting curve, defined by HREE variability, e.g., Wittig et al. (2008) (Fig. 8A). Bulk rock HREE concentration for 6 out of 8 peridotites is low and indicates between 20 and > 25% melting in the spinel stability field (Fig. 8B), which shows that the signature of melt depletion was still retained by most of our samples, though not as extensive as the 40% melt depletion usually invoked for typical cratonic peridotites (Pearson and Wittig 2008).

Metasomatism of the Elliot Lake mantle lithosphere

All Elliot Lake peridotite xenoliths have elevated Al_2O_3, TiO_2, and CaO concentrations, extending to > 6 wt.% CaO and 0.35 wt.% TiO_2, well above PUM. These values form a mixing trend between melt-depleted compositions that would be expected for the average cratonic xenolith and the lamprophyre host (Fig. 7A and B), indicating some degree of melt depletion with up to 40% mixing with the lamprophyre melt at depth for the most depleted samples (Fig. 7). This estimate is a maximum, as many of the peridotites were likely not as depleted as typical cratonic peridotites. In addition, there may have been prior metasomatic events that also incrementally increased Al, Ca, Ti, and trace elements. This metasomatic overprint has also clearly affected the HSE concentrations and ratios with a significant enrichment in Re in all samples, probably due the addition of metasomatic base metal sulfide (BMS; Luguet and Pearson 2019) and/or the lamprophyre host infiltration (cryptic). The presence of BMS cannot be confirmed with the current analyses.

Mineral trace element data from the xenoliths also highlights element correlation that could hint towards external processes affecting the samples. For example, variations of Al, Ca, Cr, V, and Na in olivine could be linked to temperature variation (De Hoog et al. 2010) or metasomatism, while variation in Ti, Y, and metals would be correlated to metasomatism. From mineral compositions and modal abundances, we recalculated the whole rock composition of our xenolith samples (ESM_1). The calculation shows variations that cannot be attributed to a specific mineral (for example, phlogopite could explain the enrichment in K in the measured samples but would add too much Mg in the calculated result compared to what is actually measured). Moreover, only a few samples show visual evidence of metasomatism in the form of intragranular serpentinite. Therefore, the metasomatism is qualified as cryptic. In the trace element diagrams constructed from the clinopyroxene data

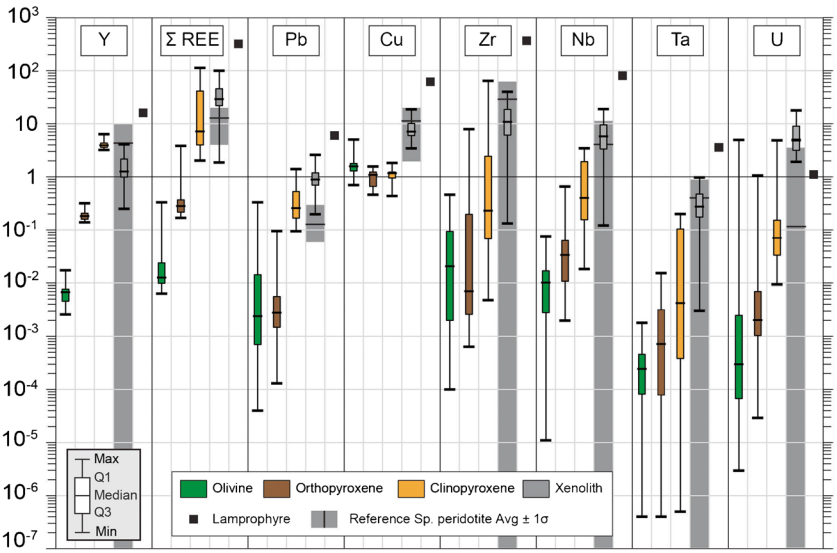

Fig. 11 Whole-rock (WR) and mineral (Ol, Opx, Cpx) metal concentrations in mantle xenoliths and their lamprophyre host (Elliot Lake, Canada). All data are expressed in ppm and are displayed as box plots with the minimum value, first quartile (25%), median, third quartile (75%), and maximum value. All WR concentrations plot are at the upper limit, or even exceed the previously reported values from spinel peridotites (McDonough 1990). The color scheme is as illustrated in Fig. 4

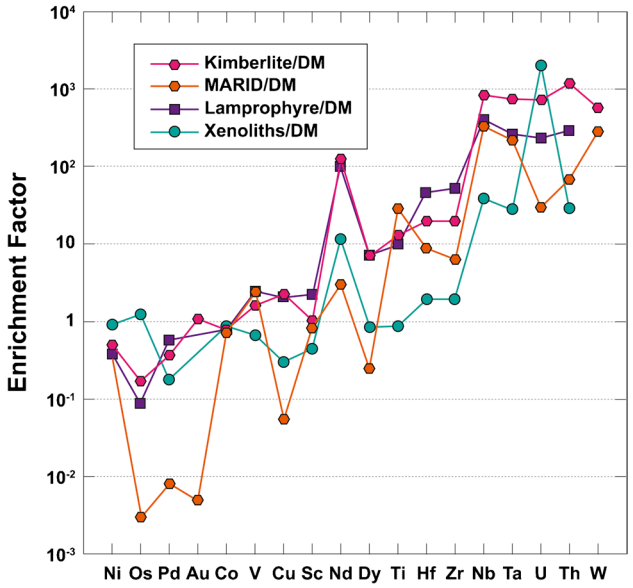

Fig. 12 Enrichment factor of kimberlites, MARID rocks (Pearson and Nowell 2002), the lamprophyre, and mantle xenoliths from Elliot Lake (this study) compared to the reference depleted mantle (DM) value of Salters and Stracke (2004)

(Fig. 5C and D), samples can be divided into two groups associated with different metasomatism types. The low Ti/Eu group is affected by carbonatitic metasomatism, while the high Ti/Eu group was metasomatised by melts that were more SiO_2-rich, likely precipitating silicates such as clinopyroxene (Fig. 5C). However, in every other diagram, the two groups plot along mixing lines with the lamprophyre host composition, which is enriched in both SiO_2 and CaO compared to Archean cratonic peridotites (Table 1). Therefore, we consider metasomatism by melts with a continuum in composition, on the silico-carbonatite to carbonated silicate melt spectrum, seen in other cratonic xenolith suites (Ionov et al. 2018), but in detail we cannot determine whether there is a single or multiple events from our observation and no indication was found in the current literature. As MgO contents in the metasomatised peridotites remain high, the melt was likely Mg-rich too.

The host lamprophyre of the Elliot Lake mantle xenoliths has a similar composition to the bulk melt inclusion compositions of silicate-carbonate globules found in xenoliths from the Slave craton in Canada (van Achterbergh et al. 2004; Bussweiler et al. 2016)—melts formed at the base of the lithosphere. In specific P–T conditions, this type of melt would intersect the silicate-carbonate solvus and unmix into conjugate silicate and carbonatite melts (Brooker and Kjarsgaard 2011). Immiscibility has not been documented in the specific area of Elliot Lake; however, the lamprophyre melt appears to be related to small degree melt compositions related to kimberlite and carbonatite melts temporally and spatially associated with the MCR rifting magmatism (Doucet et al. 2002). It is likely that the Keweenawan plume and related rifting event generated enough advective heat in the lithosphere to encourage the circulation and creation of melts such as the lamprophyre melt observed at Elliot Lake. These circulations enhanced the concentration of specific elements of economic interest like Nb-U-REE. During eruption, the enriched lamprophyre infiltrated the lithospheric mantle and grabbed pieces on its way to the crust. Moreover, the elevated initial Sr isotope composition of the lamprophyre (Fig. 10) is related to an earlier subduction event that introduced material into the base of the lithosphere, prior to the MCR event.

The cryptic infiltration of the lamprophyre host melt into the mantle peridotites is correlated to an enrichment in Ti, V, Rb, Sr, Ba, Hf and metals such as Cu, Ga, Y, Zr, Nb, Sn, Ta, Pb and REE (Figs. 4, 11, and 12; Table 1 and 2).

Carbonated melts and carbonatites are known to be related to REE and rare metal deposits through the crystallization of REE fluorcarbonates and phosphates, rich in LREE and pyrochlore (Wang et al. 2020; Yaxley et al. 2022). While REE- and Nb minerals were not observed in the Elliot Lake samples, the xenolith minerals and specifically the clinopyroxenes within the peridotites show enrichment in HFSE metals and extreme LREE/HREE fractionation (Figs. 4 and 6) and show considerable enrichments over depleted mantle.

Age of the superior mantle beneath the Elliot Lake area

Constraining the age of the mantle sampled by the ~ 1.1 Ga Elliot Lake lamprophyre is key to understanding the formation and evolution of the SCLM beneath the southern Superior Craton. Using the Re-Os system, robust model ages can be obtained for melt-depleted mantle peridotites (Shirey and Walker 1998).

A few Elliot Lake mantle xenoliths (e.g., sample 3) have low Pt and Pd concentrations that are within the range of typical melt-depleted Archean cratonic peridotites, while metasomatic re-enrichment of Re is pervasive throughout the sample suite (Fig. 9). Because Re is uniformly enriched relative to Pd, with peridotite 2a being higher in Re than the host lamprophyre, T_{MA} model ages, which assume a single-stage of Re-Os evolution, are not applicable to these peridotites. This is confirmed by the observation that only 2 of 8 peridotites give T_{MA} ages that are geologically viable (2b and 3). Instead, we can assume that most of the Re-enrichment occurred at the time of lamprophyre eruption and calculate Re-depletion ages at 1113 Ma (age of eruption, i.e., T_{RD} (erupt) ages; Pearson et al. 1995). Using this approach, we find that 4 of 8 peridotites yield Re depletion ages between 1485 and 3574 Ma (Table 1). While this could indicate that some vestiges of Archean lithospheric mantle remained beneath Elliot Lake, it is important to consider other data, such as our whole-rock analyses, which indicate extensive major and trace element addition related to the eruption of the lamprophyre host. Therefore, while these samples could potentially be Archean in origin, the Re depletion model ages have to be considered with caution and we interpret their Os isotopic signature as being strongly influenced by the MCR event and entrainment by the host lamprophyre. A similar case was observed in the clinopyroxene from Kirkland Lake (in the same geological province, 250 km NE from Elliot lake) where metasomatism at that time reset the Pb isotope ratios (Lawley et al. 2018). The MCR event is by far the most significant post-Archean lithospheric disturbance in the southern Superior craton. It is clearly visible in seismic, gravimetric and magnetic maps (Schaeffer and Lebedev 2014; Stein et al. 2018) and invoked as a significant influence on mantle Os isotope systematics as far north as the Attawapiskat kimberlite field (Smit et al. 2014).

Mesoproterozoic lithospheric geotherm beneath the Elliot Lake area

Pressures and temperatures (ESM_7) for the Elliot Lake xenoliths were calculated with the PTEXL spreadsheet (Stachel 2022) using a combination of geothermobarometers suitable for spinel peridotites. As metasomatism is prevalent in the Elliot Lake sample suite (Fig. 6), thermobarometry does not only provide estimates of "equilibration" conditions, but it can also be used to assess the extent of disequilibrium between minerals.

A simplified error propagation was carried out for pressure and temperature calculations using assumed P–T conditions (ESM_7). Errors associated with the precision of the geothermobarometer calibration are listed in Taylor (1998). Additional uncertainties can result from the chemical heterogeneity of the mineral phases. The range of measured mineral compositions was used to produce a wide array of P–T estimates, for which the average standard deviation (2σ) was calculated. Lastly, as most of the selected thermobarometers include a pressure or temperature term, the uncertainties related to input parameters were estimated by shifting them between 20 and 25 kbar and 800 and 1000 °C.

To evaluate disequilibrium in the Elliot Lake peridotites, we compared temperatures calculated for six geothermometers (Brey and Köhler 1990; Nimis and Taylor 2000; De Hoog et al. 2010; Nimis and Grütter 2010; Coogan et al. 2014; Bussweiler et al. 2017) at a fixed P–T of 25 kbar (ESM_7). This approach yields temperatures and pressures between 760 and 1100 °C. Intra-sample variation between pairs of selected mineral exchange thermometers (ΔT) ranges from below 10 °C to more than 270 °C. For samples where the temperature difference exceeds 90 °C, disequilibrium is assumed. For most peridotites, these conditions ($\Delta T > 90$ °C) are met for at least one thermometer pair, hinting at a partial disequilibrium in the Elliot Lake peridotite assemblages. Samples showing the best equilibrium results (3, 6b, and 6c) yield temperatures of 860–1100 °C and pressures of 21–33 kbar, for assumed P–T conditions of 25 kbar and 1000 °C, consistent with the variability of the whole dataset.

It is interesting to note that three thermometers based on Al concentration in olivine (calibrated for garnet-facies, De Hoog et al. 2010; Bussweiler et al. 2017; and spinel facies, Coogan et al. 2014) were compared to each other and show temperature differences of > 100 °C for a single sample and vary between ca. 800 and 1100 °C in the suite as a whole. The large range can likely be attributed to the Al concentration variability observed within olivine from a single sample (Fig. 5A).

Using the previously discussed inter-mineral equilibrium tests, we selected three thermometer-barometer

combinations to calculate equilibration conditions (ESM_7). Only a limited number of barometers are available for spinel-facies peridotites. Based on experiments by D'Souza et al. (2020), reliable P–T estimates can be obtained by combining the Ca-exchange olivine/clinopyroxene barometer (P_{KB90}, Köhler and Brey 1990) with the pressure-independent spinel-olivine exchange thermometer (T_{Co14}) of Coogan et al. (2014). Iterative calculations using the two-pyroxene (T_{BK90},Brey and Köhler 1990), or the single-clinopyroxene (T_{NT00}, Nimis and Taylor 2000) thermometers in combination with P_{KB90} also provided reasonable PT estimates.

For the whole dataset, these thermobarometer combinations yield temperatures from 850 to 1140 °C, over an estimated pressure range of 9 to 47 kbar, while results for the least disturbed samples (3, 6b, and 6c) span a much narrower range of 850–980 °C and 9–24 kbar, respectively.

On a P–T-Depth diagram (ESM_7), most samples scatter around paleogeotherms equivalent to between 50 and ~ 70 mW/m^2 crustal heat flow (Hasterok and Chapman 2011), similar to peridotites from the Vitim rift of the southern Siberian craton (Johnson et al. 2005) and significantly hotter than expected for a cratonic environment (~ 41 mW/m^2; Michaut et al. 2009). Regression of the main peridotite P/T array intercepts the mantle adiabat at approximately 130 km depth, indicating shallow depth of the cratonic root. The lithospheric mantle beneath Elliot Lake at the time of peridotite sampling has likely been thinned significantly from depths typical of cratonic roots, and was substantially thinner than the present-day average depth of the Superior cratonic root estimated at 200 km (Darbyshire et al. 2007).

Implications for metal endowment related to the MCR event

The peridotites studied here reflect metasomatism of the upper mantle beneath Elliot Lake, related to the infiltration of a silico-carbonate melt or melt close to the composition of the lamprophyre host, erupted at 1112.8 ± 4.95 Ma. This timing coincides with the initiation of the earlier stages of MCR magmatic history where the most diverse magmatism is characterized by a mix of ultramafic, mafic, alkaline and felsic melts (Heaman et al. 2007) that likely reflect significant lithospheric depth variations, induced by rifting. Previous studies have described the emplacement of mafic, ultramafic and alkaline intrusions between 1115 and 1110 Ma in the Lake Superior area, sub-coevally to the formation of some major Nb-REE deposits such as the syenite of the Coldwell complex or the Nemegosenda carbonatite (1105–1109 Ma; Heaman et al. 2007). This episode of alkaline magmatism and related HFSE mineralization is coeval to the emplacement of the Elliot Lake lamprophyre and likely shares the same source of metal enrichment as observed in our study (Sect. 8.2), with a potential deep lithospheric source for these metals, enhanced by silicate-carbonatitic metasomatic processes related to the lamprophyre melting event.

Midcontinent Rift magmatism has been documented across a large area known as the Keweenawan LIP, with a greater volume focused at the center of the rift, which coincides with Lake Superior in Canada (Fig. 1). In the Lake Superior area, several alkaline magmatic complexes have been described such as the Coldwell complex, the Killala complex and the Prairie Lake carbonatites, which are associated with Nb-U-REE deposits. This magmatism and that of the lamprophyre melt production observed at Elliot Lake (1113 ± 2.5 Ma) could share similar mechanisms responsible for the Nb-U-REE mineralization. The coeval Coldwell alkaline complex (Lake Superior; 1108 ± 1 Ma; (Heaman and Machado 1992) and other strongly alkaline magmas are associated with a strong input of metasomatised lithospheric mantle, prior to the main phase of Keweenawan LIP magmatism (based on whole rock trace element data and Hf isotopes; Good et al. 2021; Rooney et al. 2022). The metasomatised lithospheric mantle source for these mineralized magmatic rocks could be similar to the metasomatised and thinned lithospheric mantle represented by the mantle xenoliths transported by the Elliot Lake lamprophyre.

Observations of the metasomatic style evident in the lithosphere beneath Elliot Lake are also comparable to the recent results from ultramafic xenoliths and olivine xenocrysts analyzed in the northern Slave craton, which reflect a combination of silicate and carbonate-rich metasomatism. The carbonatitic metasomatism is identified by low Ti/Eu ratios in clinopyroxene and correlates with temperatures lower than 1000 °C. Such metasomatism in the Slave craton lithosphere is clearly associated with enrichment in Nb and Ta and the most enriched source for these metals is located at a depth of ca. 140 to 110 km (Veglio et al. 2022). Similarly, olivine xenocrysts derived from the same depths range in the Kirkland Lake area (in the same geological province, 250 km NE from Elliot Lake), yield Nb concentrations of 1 ppm. Moreover, clinopyroxene xenocrysts with temperatures lower than 1000 °C from the same study also fall within the carbonatitic metasomatism field (Lawley et al. 2018). In the case of Elliot Lake, our estimates show temperatures between 850 and 980 °C and depths around ~ 130 km which could indicate that both cratons underwent similar rare metal enrichment in the mid-lithosphere and the thinning associated with the MCR event in the southern Superior craton was the trigger to transport these metals to the crust, sampling this type of metasomatically enriched horizon, enhancing the HFSE metal tenor of magmas reaching the surface, which can be subsequently up-graded by fractionation processes.

Besides the typical Nb-U-REE association, a larger group of metals in the Elliot Lake metasomatised peridotites are significantly enriched by the metasomatism/melt infiltration (as seen from mineral and whole rock compositions: Cu, Y,

Zr, Nb, Ta, Pb, REE) and some above typical values for the reference spinel peridotites and the depleted mantle (Figs. 11 and 12; from a few ppm to two orders of magnitude higher). At Elliot Lake, the lamprophyre melt has sampled peridotites from close to the base of the lithosphere at ~ 130 km. The metal enrichment of the metasomatic agent and therefore the lamprophyre itself is likely due to the partial melting and circulation of melts in the lithospheric mantle, as observed for other lamprophyres of this composition (Seifert 2008; Mahéo et al. 2009). While the presence of lamprophyres is not ubiquitous in Nb-REE deposits, other studies highlight the need for mantle metasomatism to create an enriched source for these deposits (Kogarko et al. 2010; Smith et al. 2016; Dostal 2017). However, the type of metasomatism is rarely identified. A study on Bayan Obo (North China craton), one of the largest REE deposits however invokes fluxing of carbonatite magmas rich in Nb, Th and REE by high Si subduction-derived fluids, which leached Fe, Mg from the mantle wedge (Ling et al. 2013). The overall chemistry of these components is very similar to what we identified in the southern Superior craton and could indicate that silico-carbonate metasomatism, as observed in our study, is necessary to metal endowment at depth and the subsequent creation of these deposits.

On a broader level, we can examine the potential importance of small degree melts sourced either from the lithosphere or asthenosphere, and the metasomes that they produce, by comparing the enrichment factors of these melts and metasomatised lithospheric rocks to metal concentrations present in the depleted mantle (Fig. 12). The depleted mantle represents the endmember without any enrichment, and functions as a baseline against which enrichment can be evaluated. On the other side, the mica-amphibole-rutile-ilmenite-diopside (MARID) metasomatic assemblage, a heavily metasomatised rock found as xenoliths, and kimberlites, represent a sort of maximum enrichment endmembers. Finally we compare those to the average metal concentrations in the metasomatised Elliot Lake peridotites and the lamprophyre from this study. It is clear that these metasomes record little evidence of significant enrichment in base and precious metals and that small degree melts such as kimberlites or the Elliot Lake lamprophyre play little role in enriching the lithosphere with these element groups (e.g. Co, Ni, Cu, Pd, Os, Au). However, metals such as Zr, Nb, Hf and Ta, along with other "critical metals" such as Nd, Dy, U and Th, are enriched by up to three orders of magnitude compared to their concentrations in the depleted or asthenospheric mantle (Fig. 12). Such enrichments make a strong case for a central role of metasomatised lithospheric mantle acting as a source or a trap for these critical metals, which can be re-mobilized by tectono-thermal events such as the MCR or other major rifts, which disrupt lithospheric mantle and facilitate the transfer of critical metals into Earth's crust.

Ore deposit formation is complex and requires several steps of efficient concentration processes. While in most cases, only the last steps of deposition are observable, the concept of pre-enriched sources is approached in many studies over several deposit types. Specifically, magmatic ore deposits are generally issued from the selective melting of a variably enriched crustal or mantle source (Heinrich and Candela 2014). For example, in the case of porphyry and epithermal deposits, the system is sourced by the deep melting of the subducting slab beneath an active margin. But several studies suggest that the largest deposits of these types are related to pre-conditioning of the lithospheric mantle by metasomatic processes prior to hydrous melting (Pettke et al. 2010; Richards 2011). Similar models are drawn for Carlin-type deposits (Muntean et al. 2011), Mo deposits (Heinrich and Candela 2014), Nb-rich alkali systems (Mungall 2014), carbonatitic deposits (Banks et al. 2019), magmatic Ni-Cu deposits (Griffin et al. 2013), kimberlite diamond deposits (Kjarsgaard et al. 2022) and sedimentary basin deposits (Lawley et al. 2022). Further study of mantle metasomes and small-degree mantle melts containing lithospheric components is clearly needed to fully explore the links between deep pre-enriched sources and crustal ore deposits.

Conclusion

Mantle peridotite xenoliths from Elliot Lake, Ontario, give a unique insight into the metal endowment of the lithospheric mantle in the southern part of the Superior craton, on the east margin of the Mid Continent Rift ~ 1.1 Ga event. The Elliot Lake lamprophyre erupted mantle peridotite xenoliths at 1113 Ma, during the most intense stage of the MCR magmatism. Peridotite Re depletion model ages span from 1.4 to 3.5 Ga, indicating a likely significant disruption of the cratonic mantle root. The peridotites document a hot geotherm reflecting the thinning of the Superior cratonic root to ~ 130 km deep. The thinning is associated with the Keweenawan plume which created enough advective heat flow to form carbonate–silicate melts, which re-concentrated elements of economic interest. Mineral trace element systematics show a specific endowment in Nb-U-REE (up to two orders of magnitude) in the lower SCLM at the time of magmatism beneath the Elliot Lake area, linked to carbonate–silicate melt circulation. The occurrence of Mesoproterozoic alkaline complexes economically endowed with these elements is well-documented in the surrounding Lake Superior region, but this study documents the first evidence of this type of metal enrichment of the SCLM north of Lake Huron, on the east margin of the rift. We show that small-degree melts such as kimberlites or lamprophyres are very effective for transferring critical metals into the lithosphere

and that mantle metasomes and metasomatised peridotites such as those present at Elliot Lake possess several levels of magnitude of enrichments in critical metals compared to estimates of depleted mantle. As such, the lithospheric mantle likely plays a key role as a source and staging-post for the economic endowment of some critical metals in cratonic settings.

Supplementary Information The online version contains supplementary material available at https://doi.org/10.1007/s00126-023-01214-7.

Acknowledgements This contribution forms publication number MERC-ME-2023-22 for the CFREF METAL EARTH project.

Author contribution Hélène Legros: leader of project; Hélène Legros, Janina Czas, and Graham Pearson: writing of the manuscript; Yan Luo: LA-ICP-MS data acquisition; Sarah Woodland: PGE chemistry acquisition; Chiranjeeb Sarkar: Rb–Sr dating; Steven B. Shirey and Dan Schultze: sampling; All authors: revision of the manuscript.

Declarations

Conflict of interest The authors declare no competing interests.

References

Agranier A, Lee C-TA (2007) Quantifying trace element disequilibria in mantle xenoliths and abyssal peridotites. Earth Planet Sci Lett 257:290–298

Banks GJ, Walter BF, Marks MAW, Siegfried PR (2019) A workflow to define, map and name a carbonatite-or alkaline igneous-associated REE-HFSE mineral system: a case study from SW Germany. Minerals 9:97

Becker H, Horan MF, Walker RJ et al (2006) Highly siderophile element composition of the Earth's primitive upper mantle: constraints from new data on peridotite massifs and xenoliths. Geochim Cosmochim Acta 70:4528–4550. https://doi.org/10.1016/j.gca.2006.06.004

Bekker A, Kaufman AJ (2007) Oxidative forcing of global climate change: a biogeochemical record across the oldest Paleoproterozoic ice age in North America. Earth Planet Sci Lett 258:486–499

Bennett G, Dressler BO, Robertson JA, et al (1991) The Huronian Supergroup and associated intrusive rocks. In: Thurston PC, Williams HR, Sutcliffe RH, Stott GM (Eds) Geology of Ontario, vol 4. Ontario Geological Survey Special, pp 549–591

Bergen L, Fayek M (2012) Petrography and geochronology of the Pele Mountain quartz-pebble conglomerate uranium deposit, Elliot Lake District, Canada. Am Mineral 97:1274–1283

Bornhorst TJ, Mathur R (2017) Copper isotope constraints on the genesis of the Keweenaw Peninsula native copper district, Michigan, USA. Minerals 7:185

Boyd FR, Pokhilenko NP, Pearson DG et al (1997) Composition of the Siberian cratonic mantle: evidence from Udachnaya peridotite xenoliths. Contrib to Mineral Petrol 128:228–246

Brey GP, Köhler T (1990) Geothermobarometry in four-phase lherzolites II. New thermobarometers, and practical assessment of existing thermobarometers. J Petrol 31:1353–1378

Brooker RA, Kjarsgaard BA (2011) Silicate–carbonate liquid immiscibility and phase relations in the system SiO2–Na2O–Al2O3–CaO–CO2 at 0·1–2·5 GPa with applications to carbonatite genesis. J Petrol 52:1281–1305. https://doi.org/10.1093/petrology/egq081

Bussweiler Y, Stone RS, Pearson DG et al (2016) The evolution of calcite-bearing kimberlites by melt-rock reaction: evidence from polymineralic inclusions within clinopyroxene and garnet megacrysts from Lac de Gras kimberlites, Canada. Contrib to Mineral Petrol 171:1–25

Bussweiler Y, Brey GP, Pearson DG et al (2017) The aluminum-in-olivine thermometer for mantle peridotites—experimental versus empirical calibration and potential applications. Lithos 272:301–314

Bussweiler Y, Pearson DG, Stachel T, Kjarsgaard BA (2018) Cr-rich megacrysts of clinopyroxene and garnet from Lac de Gras kimberlites, Slave Craton, Canada–implications for the origin of clinopyroxene and garnet in cratonic lherzolites. Mineral Petrol 112:583–596

Bussweiler Y, Giuliani A, Greig A et al (2019) Trace element analysis of high-Mg olivine by LA-ICP-MS–characterization of natural olivine standards for matrix-matched calibration and application to mantle peridotites. Chem Geol 524:136–157

Castor SB (2008) Rare earth deposits of North America. Resour Geol 58:337–347. https://doi.org/10.1111/j.1751-3928.2008.00068.x

Coltorti M, Bonadiman C, Hinton RW et al (1999) Carbonatite metasomatism of the oceanic upper mantle: evidence from clinopyroxenes and glasses in ultramafic xenoliths of Grande Comore, Indian Ocean. J Petrol 40:133–165

Coogan LA, Saunders AD, Wilson RN (2014) Aluminum-in-olivine thermometry of primitive basalts: evidence of an anomalously hot mantle source for large igneous provinces. Chem Geol 368:1–10

Darbyshire FA, Eaton DW, Frederiksen AW, Ertolahti L (2007) New insights into the lithosphere beneath the Superior Province from Rayleigh wave dispersion and receiver function analysis. Geophys J Int 169:1043–1068

De Hoog JCM, Gall L, Cornell DH (2010) Trace-element geochemistry of mantle olivine and application to mantle petrogenesis and geothermobarometry. Chem Geol 270:196–215

Dostal J (2017) Rare earth element deposits of alkaline igneous rocks. Resources 6:34

Doucet P, Moorhead J, Côté S (2002) Chapter 1C Southern Superior Province (Abitibi and Pontiac Subprovinces). In: The Abitibi subprovince, vol 16. Gouvernement du Québec

Easton RM, Thurston PC (1992) The Grenville Province and the Proterozoic history of central and southern Ontario. Geol Ontario Spec 4:714–904

Edwards GH, Blackburn T (2018) Detecting the extent of ca. 1.1 Ga Midcontinent Rift plume heating using U-Pb thermochronology of the lower crust. Geology 46:911–914. https://doi.org/10.1130/G45150.1

Eggins SM, Rudnick RL, McDonough WF (1998) The composition of peridotites and their minerals: a laser-ablation ICP–MS study. Earth Planet Sci Lett 154:53–71

Fedo CM, Wayne Nesbitt H, Young GM (1995) Unraveling the effects of potassium metasomatism in sedimentary rocks and paleosols, with implications for paleoweathering conditions and provenance. Geology 23:921–924

Fischer-Gödde M, Becker H, Wombacher F (2011) Rhodium, gold and other highly siderophile elements in orogenic peridotites and peridotite xenoliths. Chem Geol 280:365–383

Frarey MJ (1978) Geology of the Huronian belt between Sault Ste. Marie and Blind river, Ontario. Geological Survey of Canada report 383:87

Geusebroek PA, Duke NA (2004) An update on the geology of the Lupin gold mine, Nunavut, Canada. Explor Min Geol 13:1–13. https://doi.org/10.2113/gsemg.13.1-4.1

Good DJ, Hollings P, Dunning G et al (2021) A new model for the Coldwell complex and associated dykes of the Midcontinent Rift. Canada J Petrol 62:036

Griffin WL, Begg GC, O'reilly SY (2013) Continental-root control on the genesis of magmatic ore deposits. Nat Geosci 6:905–910

Groves DI, Santosh M (2021) Craton and thick lithosphere margins: the sites of giant mineral deposits and mineral provinces. Gondwana Res 100:195–222. https://doi.org/10.1016/j.gr.2020.06.008

Hasterok D, Chapman DS (2011) Heat production and geotherms for the continental lithosphere. Earth Planet Sci Lett 307:59–70

Heaman LM, Machado N (1992) Timing and origin of midcontinent rift alkaline magmatism, North America: evidence from the Coldwell complex. Contrib to Mineral Petrol 110:289–303

Heaman LM, Easton RM, Hart TR et al (2007) Further refinement to the timing of Mesoproterozoic magmatism, Lake Nipigon region, Ontario. Can J Earth Sci 44:1055–1086

Heinrich CA, Candela PA (2014) Fluids and ore formation in the Earth's crust. In: Treatise on geochemistry (second edition), vol 13. Elsevier, pp 1–28

Hoffman PF, Bally AW, Palmer AR (1989) Precambrian geology and tectonic history of North America. The geology of North America—an overview. Geological Society of America Boulder, CO, pp 447–512

Ionov DA, Doucet LS, Xu Y et al (2018) Reworking of Archean mantle in the NE Siberian craton by carbonatite and silicate melt metasomatism: evidence from a carbonate-bearing, dunite-to-websterite xenolith suite from the Obnazhennaya kimberlite. Geochim Cosmochim Acta 224:132–153. https://doi.org/10.1016/j.gca.2017.12.028

Johnson JS, Gibson SA, Thompson RN, Nowell GM (2005) Volcanism in the Vitim volcanic field, Siberia: geochemical evidence for a mantle plume beneath the Baikal rift zone. J Petrol 46:1309–1344

Kjarsgaard BA, de Wit M, Heaman LM et al (2022) A review of the geology of global diamond mines and deposits. Rev Mineral Geochemistry 88:1–117. https://doi.org/10.2138/rmg.2022.88.01

Kogarko LN, Lahaye Y, Brey GP (2010) Plume-related mantle source of super-large rare metal deposits from the Lovozero and Khibina massifs on the Kola Peninsula, Eastern part of Baltic Shield: Sr, Nd and Hf isotope systematics. Mineral Petrol 98:197–208. https://doi.org/10.1007/s00710-009-0066-1

Lawley CJM, McCafferty AE, Graham GE et al (2022) Data–driven prospectivity modelling of sediment–hosted Zn–Pb mineral systems and their critical raw materials. Ore Geol Rev 141:104635. https://doi.org/10.1016/j.oregeorev.2021.104635

Lawley CJM, Kjarsgaard BA, Jackson SE et al (2018) Olivine and clinopyroxene mantle xenocryst geochemistry from the Kirkland Lake kimberlite field. Ontario, Geological Survey of Canada report, p 8376

Lightfoot PC (2017) Chapter 2 - A synthesis of the geology of the Sudbury Structure. In: Nickel sulfide ores and impact melts, Elsevier, pp 68–189

Ling M-X, Liu Y-L, Williams IS et al (2013) Formation of the world's largest REE deposit through protracted fluxing of carbonatite by subduction-derived fluids. Sci Rep 3:1776. https://doi.org/10.1038/srep01776

Long DGF, Ulrich T, Kamber BS (2011) Laterally extensive modified placer gold deposits in the Paleoproterozoic Mississagi Formation, Clement and Pardo Townships, Ontario. Can J Earth Sci 48:779–792

Long DGF (1986) Stratigraphic and depositional setting of placer gold concentrations in basal Huronian strata of the Cobalt Plain. Ontario Geological Survey report, p 5593

Lougheed HD, McClenaghan MB, Layton-Matthews D, Leybourne M (2020) Exploration potential of fine-fraction heavy mineral concentrates from till using automated mineralogy: a case study from the Izok Lake Cu–Zn–Pb–Ag VMS deposit, Nunavut. Canada Minerals 10:310. https://doi.org/10.3390/min10040310

Luguet A, Pearson G (2019) Dating mantle peridotites using Re-Os isotopes: the complex message from whole rocks, base metal sulfides, and platinum group minerals. Am Mineral J Earth Planet Mater 104:165–189

Luguet A, Nowell GM, Pearson DG (2008) 184Os/188Os and 186Os/188Os measurements by negative thermal ionisation mass spectrometry (N-TIMS): effects of interfering element and mass fractionation corrections on data accuracy and precision. Chem Geol 248:342–362. https://doi.org/10.1016/j.chemgeo.2007.10.013

Mahéo G, Blichert-Toft J, Pin C et al (2009) Partial melting of mantle and crustal sources beneath South Karakorum, Pakistan: implications for the Miocene geodynamic evolution of the India-Asia convergence zone. J Petrol 50:427–449

Martindale RD (1968) The concentration and distribution of gold in the uraniferous conglomerates of Elliot Lake. Dissertation, McMaster University, p 132

McDonough WF (1990) Constraints on the composition of the continental lithospheric mantle. Earth Planet Sci Lett 101:1–18

McDonough WF, Sun S-S (1995) The composition of the Earth. Chem Geol 120:223–253

Michaut C, Jaupart C, Mareschal J-C (2009) Thermal evolution of cratonic roots. Lithos 109:47–60. https://doi.org/10.1016/j.lithos.2008.05.008

Miller JD, Nicholson SW, Easton RM et al (2013) Geology and mineral deposits of the 1.1 Ga Midcontinent rift in the Lake Superior Region—an overview. F Guid to Copper-Nickel-Platinum Gr Elem Depos Lake Super Reg Ed by Miller, J Precambrian Res Cent Guideb 13:1–49

Montsion RM, Thurston P, Ayer J (2018) 1: 2 000 000 scale geological compilation of the Superior craton - Version 1: Mineral Exploration Research Centre, Harquail School of Earth Sciences, Laurentian University Document Number MERC-ME-2018-017

Mossman DJ, Harron GA (1983) Origin and distribution of gold in the Huronian Supergroup, Canada—the case for Witwatersrand-type paleoplacers. In: Developments in Precambrian geology, vol 7. Elsevier, pp 435–475

Mungall JE (2014) Chapter 13.8 Geochemistry of magmatic ore deposits. In: Treatise on geochemistry, 2nd edn. pp 195–215

Muntean JL, Cline JS, Simon AC, Longo AA (2011) Magmatic–hydrothermal origin of Nevada's Carlin-type gold deposits. Nat Geosci 4:122–127. https://doi.org/10.1038/ngeo1064

Nicholson SW, Shirey SB (1990) Midcontinent rift volcanism in the Lake Superior region: Sr, Nd, and Pb isotopic evidence for a mantle plume origin. J Geophys Res Solid Earth 95:10851–10868

Nicholson SW, Cannon WF, Schulz KJ (1992) Metallogeny of the Midcontinent rift system of North America. Precambrian Res 58:355–386

Nimis P, Grütter H (2010) Internally consistent geothermometers for garnet peridotites and pyroxenites. Contrib to Mineral Petrol 159:411–427

Nimis P, Taylor WR (2000) Single clinopyroxene thermobarometry for garnet peridotites. Part I. Calibration and testing of a Cr-in-Cpx barometer and an enstatite-in-Cpx thermometer. Contrib to Mineral Petrol 139:541–554

Norman DI (1978) Ore deposits related to the Keweenawan rift. In: Petrology and geochemistry of continental rifts : Volume One of the Proceedings of the NATO Advanced Study Institute Paleorift Systems with Emphasis on the Permian Oslo Rift, held in Oslo,

Norway, July 27–August 5, 1977. Dordrecht: Springer, Netherlands, pp 245–253
O'Reilly SY, Griffin WL (2013) Mantle metasomatism. In: Metasomatism and the chemical transformation of rock. Lecture Notes in Earth System Sciences. Springer, Berlin, Heidelberg. https://doi.org/10.1007/978-3-642-28394-9_12
Ono S, Fayek M (2011) Decoupling of O and Pb isotope systems of uraninite in the early Proterozoic conglomerates in the Elliot Lake district. Chem Geol 288:1–13. https://doi.org/10.1016/j.chemgeo.2010.03.015
Ottley CJ, Pearson DG, Irvine GJ (2003) A routine method for the dissolution of geological samples for the analysis of REE and trace elements via ICP-MS. In: Plasma source mass spectrometry: applications and emerging technologies, vol 288. Royal Society of Chemistry Cambridge, p 221
Paton C, Hellstrom J, Paul B et al (2011) Iolite: freeware for the visualisation and processing of mass spectrometric data. J Anal at Spectrom 26:2508–2518
Pearson DG, Nowell GM (2002) The continental lithospheric mantle: characteristics and significance as a mantle reservoir. Philos Trans R Soc London Ser A Math Phys Eng Sci 360:2383–2410
Pearson DG, Wittig N (2008) Formation of Archaean continental lithosphere and its diamonds: the root of the problem. J Geol Soc London 165:895–914. https://doi.org/10.1144/0016-76492008-003
Pearson DG, Woodland SJ (2000) Solvent extraction/anion exchange separation and determination of PGEs (Os, Ir, Pt, Pd, Ru) and Re–Os isotopes in geological samples by isotope dilution ICP-MS. Chem Geol 165:87–107
Pearson DG, Carlson RW, Shirey SB et al (1995) Stabilisation of Archaean lithospheric mantle: a ReOs isotope study of peridotite xenoliths from the Kaapvaal craton. Earth Planet Sci Lett 134:341–357. https://doi.org/10.1016/0012-821X(95)00125-V
Pearson DG, Irvine GJ, Carlson RW et al (2002) The development of lithospheric keels beneath the earliest continents: time constraints using PGE and Re-Os isotope systematics. Geol Soc London, Spec Publ 199:65–90
Pearson DG, Irvine GJ, Ionov DA et al (2004) Re–Os isotope systematics and platinum group element fractionation during mantle melt extraction: a study of massif and xenolith peridotite suites. Chem Geol 208:29–59
Pearson DG, Wittig N (2014) Chapter 3.6 - The Formation and evolution of cratonic mantle lithosphere – evidence from mantle xenoliths. In: Treatise on Geochemistry, 2nd edn. Elsevier, pp 255–292. https://doi.org/10.1016/B978-0-08-095975-7.00205-9
Pearson DG, Canil D, Shirey SB (2014) Chapter 3.5 - Mantle samples included in volcanic rocks: xenoliths and diamonds. In: Treatise on Geochemistry, 3rd edn. Elsevier, pp 169–253. https://doi.org/10.1016/B978-0-08-095975-7.00216-3
Percival JA, Skulski T, Sanborn-Barrie M et al (2012) Geology and tectonic evolution of the Superior Province, Canada. Tecton Styles Canada Lithoprobe Perspect Spec Pap 49:321–378
Pettke T, Oberli F, Heinrich CA (2010) The magma and metal source of giant porphyry-type ore deposits, based on lead isotope microanalysis of individual fluid inclusions. Earth Planet Sci Lett 296:267–277. https://doi.org/10.1016/j.epsl.2010.05.007
Potts PJ (2012) A handbook of silicate rock analysis. Springer Science & Business Media New York, p 622. https://doi.org/10.1007/978-1-4615-3270-5
Richards JP (2011) Magmatic to hydrothermal metal fluxes in convergent and collided margins. Ore Geol Rev 40:1–26. https://doi.org/10.1016/j.oregeorev.2011.05.006
Robertson JA (1976) The Blind River uranium deposits: the ores and their setting. Ontario Minist Nat Resour 8:45
Robinson A, Spooner ETC (1982) Source of the detrital components of uraniferous conglomerates, Quirke ore zone, Elliot Lake, Ontario, Canada. Nature 299:622–624
Rock NMS (1991) Lamprophyres. Springer Science+Business Media New York, p 285. https://doi.org/10.1007/978-1-4757-0929-2
Rooney TO, Konter JG, Finlayson VA et al (2022) Constraining the isotopic endmembers contributing to 1.1 Ga Keweenawan large igneous province magmatism. Contrib to Mineral Petrol. 177:49. https://doi.org/10.1007/s00410-022-01907-8
Roscoe SM (1976) Huronian rocks and uraniferous conglomerates in the Canadian Shield. Geological Survey of Canada report, pp 68–40
Rousell DH, Meyer W, Prevec SA et al (2002) Bedrock geology and mineral deposits. Spec Vol Ontario Geol Surv 5:21–55
Salters VJM, Stracke A (2004) Composition of the depleted mantle. Geochemistry, Geophys Geosystems 5. https://doi.org/10.1029/2003GC000597
Schaeffer AJ, Lebedev S (2014) Imaging the North American continent using waveform inversion of global and USArray data. Earth Planet Sci Lett 402:26–41
Scott JM, Liu J, Pearson DG, Waight TE (2016) Mantle depletion and metasomatism recorded in orthopyroxene in highly depleted peridotites. Chem Geol 441:280–291. https://doi.org/10.1016/j.chemgeo.2016.08.024
Seifert T (2008) Metallogeny and petrogenesis of lamprophyres in the Mid-European Variscides: post-collisional magmatism and its relationship to late-variscan ore forming processes in the Erzgebirge (Bohemian Massif). IOS press, p 304
Shirey SB, Walker RJ (1998) The Re-Os isotope system in cosmochemistry and high-temperature geochemistry. Annu Rev Earth Planet Sci 26:423–500
Shu Q, Brey GP (2015) Ancient mantle metasomatism recorded in subcalcic garnet xenocrysts: temporal links between mantle metasomatism, diamond growth and crustal tectonomagmatism. Earth Planet Sci Lett 418:27–39
Smit KV, Pearson DG, Stachel T, Seller M (2014) Peridotites from Attawapiskat, Canada: Mesoproterozoic reworking of Palaeoarchaean lithospheric mantle beneath the Northern Superior superterrane. J Petrol 55:1829–1863
Smith MP, Moore K, Kavecsánszki D et al (2016) From mantle to critical zone: a review of large and giant sized deposits of the rare earth elements. Geosci Front 7:315–334. https://doi.org/10.1016/j.gsf.2015.12.006
Smyk MC, Franklin JM (2007) A synopsis of mineral deposits in the Archean and Proterozoic rocks of the Lake Nipigon Region, Thunder Bay District, Ontario. Can J Earth Sci 44:1041–1053
Sproule RA, Sutcliffe R, Tracanelli H, Lesher CM (2007) Palaeoproterozoic Ni–Cu–PGE mineralisation in the Shakespeare intrusion, Ontario, Canada: a new style of Nipissing gabbro-hosted mineralisation. Appl Earth Sci 116:188–200
Stachel T (2022) Excel spreadsheet to do geothermobarometry for mantle assemblages: developments up to date and recent calibrations in geothermobarometry of mantle rocks based on the PTEXL program written by Thomas Köhler. Unpubl Work
Stein S, Van Der Lee S, Jurdy D et al (2011) Learning from failure: the SPREE mid-continent rift experiment. GSA Today 21:5–7
Stein S, Stein CA, Elling R et al (2018) Insights from North America's failed Midcontinent Rift into the evolution of continental rifts and passive continental margins. Tectonophysics 744:403–421. https://doi.org/10.1016/j.tecto.2018.07.021
Tang Y-J, Zhang H-F, Ying J-F et al (2008) Refertilization of ancient lithospheric mantle beneath the central North China Craton: evidence from petrology and geochemistry of peridotite xenoliths. Lithos 101:435–452

Taylor WR (1998) An experimental test of some geothermometer and geobaro-meter formulations for upper mantle peridotites with application to the ther-mobarometry of fertile lherzolite and garnet websterite. Neues Jahrb für Mineral 172(2–3):381–408

Ulrich T, Long DGF, Kamber BS, Whitehouse MJ (2011) In situ trace element and sulfur isotope analysis of pyrite in a paleoproterozoic gold placer deposit, Pardo and Clement Townships, Ontario, Canada. Econ Geol 106:667–686

van Achterbergh E, Griffin WL, Ryan CG et al (2004) Melt inclusions from the deep Slave lithosphere: implications for the origin and evolution of mantle-derived carbonatite and kimberlite. Lithos 76:461–474. https://doi.org/10.1016/j.lithos.2004.04.007

Veglio C, Lawley CJM, Pearson DG et al (2022) Olivine xenocrysts reveal carbonated mid-lithosphere in the northern Slave craton. Lithos 414:106633

Vermeesch P (2018) IsoplotR: a free and open toolbox for geochronology. Geosci Front 9:1479–1493

Wang Z-Y, Fan H-R, Zhou L et al (2020) Carbonatite-Related REE Deposits: an Overview Minerals 10:965

Waterton P, Pearson DG, Kjarsgaard B et al (2017) Age, origin, and thermal evolution of the ultra-fresh~ 1.9 Ga Winnipegosis Komatiites, Manitoba. Canada Lithos 268:114–130

Waterton P, Pearson DG, Mertzman SA et al (2020) A fractional crystallization link between komatiites, basalts, and dunites of the Palaeoproterozoic Winnipegosis Komatiite Belt, Manitoba. Canada J Petrol 61:052. https://doi.org/10.1093/petrology/egaa052

Waterton P, Mungall J, Pearson DG (2021) The komatiite-mantle platinum-group element paradox. Geochim Cosmochim Acta 313:214–242

Wittig N, Pearson DG, Webb M et al (2008) Origin of cratonic lithospheric mantle roots: a geochemical study of peridotites from the North Atlantic Craton, West Greenland. Earth Planet Sci Lett 274:24–33

Woodruff LG, Schulz KJ, Nicholson SW, Dicken CL (2020) Mineral deposits of the Mesoproterozoic Midcontinent Rift system in the Lake Superior region – a space and time classification. Ore Geol Rev 126:103716. https://doi.org/10.1016/j.oregeorev.2020.103716

Wu F-Y, Mitchell RH, Li Q-L et al (2017) Emplacement age and isotopic composition of the Prairie Lake carbonatite complex, Northwestern Ontario, Canada. Geol Mag 154:217–236

Wyman DA, Kerrich R (1993) Archean shoshonitic lamprophyres of the Abitibi Subprovince, Canada: petrogenesis, age, and tectonic setting. J Petrol 34:1067–1109

Yamaguchi KE, Ohmoto H (2006) Evidence from sulfur isotope and trace elements in pyrites for their multiple post-depositional processes in uranium ores at the Stanleigh Mine, Elliot Lake, Ontario. Canada Mem Soc Am 198:143

Yaxley GM, Anenburg M, Tappe S et al (2022) Carbonatites: classification, sources, evolution, and emplacement. Annu Rev Earth Planet Sci 50:261–293

Young GM (1991) Stratigraphy, sedimentology and tectonic setting of the Huronian Supergroup, Geological Association of Canada, Mineralogical Association of Canada. In: Field trip guidebook (Geological Association of Canada), B5, Geological Association of Canada, Toronto '91 Organizing Committee, Sudbury, Ont., Canada, p 34